FLUORESCENCE LIFETIME OF PDT PHOTOSENSITIZERS

FLUORESCENCE LIFETIME OF PDT PHOTOSENSITIZERS

By

Jennifer Russell, B.Eng

A Thesis

Submitted to the School of Graduate Studies

in Partial Fulfillment of the Requirements

for the Degree

Master of Applied Science

McMaster University

MASTER OF APPLIED SCIENCE (2008) McMaster University
(Biomedical Engineering) Hamilton, Ontario

TITLE: Fluorescence Lifetime of PDT Photosensitizers

AUTHOR: Jennifer Russell, B.Eng (McMaster University)

SUPERVISORS: Dr. Qiyin Fang, Dr. Joseph Hayward

NUMBER OF PAGES: x, 89

Abstract

Photodynamic therapy (PDT) is an effective treatment option for various types of invasive tumors, the efficacy of which depends strongly on selective cell uptake and selective excitation of the tumor, which relies on proper dosage. The characterization of the fluorescence lifetimes of photosensitizers localized inside living cells may provide the basis for further investigation of *in vitro* PDT dosage measurements using time-domain spectroscopy and imaging. In this thesis, the fluorescence lifetimes of localized Photofrin® and delta-aminolevulinic acid (ALA) induced protoporphyrin IX (PpIX) were investigated in living MAT-LyLu (MLL) rat prostate adenocarcinoma cells. Cells were incubated with the photosensitizers, and then treated with light under well-oxygenated conditions using a two-photon fluorescence lifetime imaging microscope (FLIM). Fluorescence lifetime images of these cells were recorded with average lifetimes of 5.5 ± 1.2 ns for Photofrin and 6.3 ± 1.2 ns for ALA-induced PpIX over 600 to 750 nm. Two channel FLIM revealed lifetimes of 7.8 ± 0.5 ns for Photofrin® and 10.8 ± 1.7 ns for PpIX over 620 to 645 nm, while photoproducts observed on the second channel yielded lifetimes of 5.1 ± 0.4 ns over 650 to 670 nm for Photofrin® and 6.3 ± 1.0 ns over 670 to 690 nm for PpIX. Fluorescence lifetimes of both photosensitizers were found to be significantly shorter when localized in cells than when measured in solutions, suggesting that photosensitizers' lifetimes go through significant changes when bonded to intracellular components. These changes in lifetime also provide opportunities to quantitatively measure and monitor the binding states of the photosensitizers and their microenvironment, which may be used in real-time PDT dosimetry, as well as for diagnostic purposes.

Acknowledgements

I would first and foremost like to express my gratitude to Dr. Qiyin Fang and Dr. Joe Hayward, under whose supervision this thesis was completed, and thank them for the guidance they have given me. I would also like to thank Dr. Kevin Diamond for his invaluable insight and input along the way, and Dr. Tony Collins for his indispensable guidance and discussions regarding cell culturing, imaging and analysis. Thanks also go to Dr. Henry Tiedje, without whom the two-photon streak camera experiments would not have been possible, Mark Weston for providing me with cells, and Jonathan Lovell for measuring the absorption-emission spectra and lifetimes using the Chronos system.

Table of Contents

List of Figures

Chapter I – Introduction and Background Information

1.1 Cancer Biology, Standard Methods of Treatment, and the Motivation Behind Photodynamic Therapy

According to the Canadian Cancer Society, based on their general cancer statistics for 2007, 3075 Canadians on average are diagnosed with cancer and 1398 Canadians die of cancer each week (Canadian Cancer Statistics 2007). Based on current incidence rates, they state that 39% of woman and 44% of men in Canada will develop cancer in their lifetimes, with the overall prevalence of cancer in Canada being around 2.5% among men and 2.8% in women. Among the most prevalent are prostate, lung and colorectal in men, and breast, lung and colorectal in women, with lung cancer dominating as the leading cancer death in both men and women. Colorectal cancer is the second leading cause of cancer-related death (Canadian Cancer Statistics 2007). Based on current mortality rates, they predict that around 1 in 4 Canadians, 24% of women and 28% of men, will die from cancer. Relative survival rates are lowest for cancers of the pancreas, esophagus, liver and lung, and highest for testicular, thyroid and prostate cancers, as well as melanomas. Around 1300 children in Canada develop cancer annually, with the mortality rate being around one sixth.

Cancer can be described as unregulated cell replication. New tissue growth may fall into one of four categories: hypertrophy, where there is an increase in cell size, yet normal organization is maintained; hyperplasia, where

there is an increase in cell number, yet normal organization is maintained; dysplasia, in which there is disorganized growth; and neoplasia, which is characterized by disorganized growth and an increase in cell number (Kleinsmith 2006). Neither hypertrophy nor hyperplasia is an indication of cancer, as they involve either the increase in size or number of normal cells, and both are potentially reversible. Areas of dysplasia may recover normal organization, or progress into neoplasia (Kleinsmith 2006). Neoplastic growth is characterized by uncontrolled proliferation, resulting in a tumour. The balance between cell division, cell differentiation and cell death is disrupted, such that there is a net increase in the number of dividing cells, contributing to the growth of the tumour (Kleinsmith 2006).

Tumour growth can be categorized as either benign or malignant. Expansion in cell numbers that is locally confined is characteristic of a benign growth, whereas invasion of surrounding tissues constitutes malignant growth (Pelengaris 2006). Benign growths are rarely life threatening since they typically grow slowly; these cells also tend to exhibit normal tissue organization with well defined boundaries and cells are characterized by regular nuclear shape and a low relative number of dividing cells. Malignant growths may progress rapidly and are often life threatening, with poorly defined margins; these cells tend to exhibit irregular nuclear shape and a high number of dividing cells (Kleinsmith 2006). Cancer is the label given to any type of malignant tumour. Six hallmarks can generally be attributed to cancer: cells exhibit self-sufficiency in growth signals,

insensitivity to antigrowth signals, anti-apoptotic properties, unlimited replicative ability, sustainable angiogenesis, and they can invade surrounding tissue and metastasize to distant sites (Kleinsmith 2006).

Cancers are classified based on the tissue of origin, independent of the afflicted organ, relying on similarities in cellular structure and tumour function. Tumours can be either liquid, like leukemias and lymphomas, composed of neoplastic cells with motile precursors; or solid, composed of epithelial or mesenchymal cells which are immobile. Pathologically, there are four classifications for cancers: carcinomas, which originate in epithelial cells in skin or in the lining of internal organs, comprising approximately 80% of human cancers; sarcomas, which originate in connective or supportive tissues such as bone, cartilage, fat, muscle and blood vessels; leukemias, which originate in bone marrow and result in the production of large numbers of abnormal blood cells; and lymphomas, which originate in cells of the immune system (Kleinsmith, Pelengaris 2006).

Cancer cells are characterized by several properties that contribute to their propensity for uncontrolled proliferation, ability to relocate to other tissues in the body, and their general lethality. One is their anchorage-independent growth. Normal cells must be anchored to the extracellular matrix before they can reproduce, and if they become detached from the extracellular matrix they will undergo apoptosis (programmed cell death), triggered by the lack of contact with the extracellular matrix. This property of normal cells safeguards against having

cells drift from their tissue of origin and begin dividing in another tissue (Kleinsmith 2006). Normal cells are therefore said to be anchorage-dependent. Cancer cells do not exhibit this property, thus they can divide whether anchored or not, and they are free to drift to distant sites in the body where they can continue dividing (Kleinsmith 2006). Normal cells also exhibit a finite lifespan, determined by the shortening of the telomeres of each chromosome with successive cell divisions. When the telomeres become so short that they are not able to bind telomere capping proteins or loop in on themselves, a bare end of DNA is exposed, which is unstable. Unprotected ends of DNA may bind together, and the chromosomes fragment and separate improperly during division (Kleinsmith 2006). Normal cells have a safeguard against this, as unprotected ends of DNA trigger apoptosis. Some cells, however, must retain the ability to divide for a very long time, such as bone marrow cells, which need to constantly produce new blood cells. Cells like these produce telomerase, which constantly adds new copies of the telomeric sequence to the ends of chromosomes, so these cells can divide indefinitely (Kleinsmith 2006). Most cancer cells are able to activate the telomerase gene and use this mechanism to confer immortality upon themselves. Some cancer cells employ another mechanism to preserve their telomeres, but regardless of the method, the result is the ability to divide indefinitely (Kleinsmith 2006). Other characteristics of cancer cells include: their independence from the need for stimulation by external growth factors (either by producing their own growth factors or possessing mutated growth factor receptors

that are always activated), gross chromosomal abnormalities, the absence of functional cell cycle checkpoints (which, in a normal cell, would recognize DNA damage and halt division), and their ability to evade apoptosis through various mechanisms such as disabling genes which code for proteins involved in the apoptotic pathway (Kleinsmith 2006).

One of the first steps in tumour metastasis, the relocation of tumour tissue to other sites in the body, is the recruitment of blood vessels that feed into the tumour and supply it with oxygen and nutrients. Without a network of blood vessels, a tumour could not grow larger than a few millimeters in size (Kleinsmith 2006). Tumour feeding blood vessels are recruited via angiogenesis, a process by which new blood vessels sprout from existing vessels. This process is a necessary part of embryo development. Tumours accomplish this by secreting two proteins: vascular endothelial growth factor and fibroblast growth factor, which promotes angiogenesis. Metastasis occurs once cancer cells enter the bloodstream or lymphatic system and are carried to other sites in the body where they can invade the new tissue site (Kleinsmith 2006).

Early detection and treatment provide the best chance for a positive outcome for the patient, thus screening tools designed to identify premalignant and early-stage lesions are very important. Once the presence of cancer has been identified, treatment can begin. Presently, the most common methods of cancer treatment include chemotherapy, radiation therapy, and surgery. Chemotherapy is a systemic treatment, and as such it affects fast-dividing cells throughout the

body, regardless of whether they are cancerous or healthy, and it is well known to cause negative side effects in many patients (American Cancer Society 2007). Radiation therapy, though more localized, can also cause severe adverse side effects as it weakly discriminates between cancerous and healthy tissue. Surgical removal of the tumour is an invasive treatment option that incorporates the usual risks associated with surgery, and it is often followed by radiation or chemotherapy (American Cancer Society 2007). Depending on the location and nature of the tumour, surgical removal may not even be possible.

As previously mentioned, chemotherapy is not tumour specific, but rather targets all cells that are dividing rapidly. This includes normal cells such as those contained in hair follicles and cells of the gastrointestinal mucosa (Thomas 2006). Treatments are given intermittently, with the shortest possible time between treatments that allows for normal tissue, such as bone marrow and GI tissue, to experience some recovery. Tumour cells tend to take longer to recover from cytotoxic damage than normal cells, so each successive treatment should deplete the tumour cell population. Chemotherapy is most often used to treat advanced cancer, to reduce the volume of solid tumours, or in adjunct with surgery or radiation once the primary tumour has been controlled (Thomas 2006).

Radiotherapy employs ionizing radiation like X-rays, gamma rays, and electron beams to deposit energy in tissue through excitation and ionization events (Thomas 2006), resulting in apoptotic or mitotic death (the inability of a cell to divide due to extensive chromosomal damage) in both cancer cells and

normal cells alike (Kleinsmith 2006). Radiation is delivered to the target malignant tissue with the intention of inflicting minimal damage to normal surrounding tissue. Dose is measured in units of Grays (Gy), where 1 Gy is equivalent to 1 Joule of energy per kilogram of mass. Several different delivery schemes are currently employed. X-ray tubes produce 80-300 kV X-rays and are mostly used in the treatment of skin cancer and palliative treatment for skin and bone metastases (Thomas 2006). Cobalt teletherapy machines produce two gamma rays per disintegration with an average energy of 1.2 MeV, though they have largely been replaced by linear accelerators, which use electrons accelerated to high energies to bombard a tungsten target to produce 4-25 MV X-rays. These high energy photon beams are used to treat deep seated tumours. Removing the tungsten target permits treatment with electrons. As they only penetrate a short distance, they are used primarily for skin and lip treatments (Thomas 2006). Radiation can also be placed directly into the tumour, through a procedure called brachytherapy. Radioactive sources such as cesium-137, iodine-125, or iridium-192 are most typically used for treatment inside cavities (*e.g.* uterus), or interstitially (*e.g.* prostate). Systemic radiation therapy involves an oral or injected dose of an unsealed source, an example of which is the oral administration of iodine-131 for treatment of thyroid cancer (Thomas 2006). The degree of damage sustained by normal tissue is related to the rate of turnover of cells in that tissue. Cells with a fast turnover rate like epithelial cells will exhibit acute effects over days to weeks, while cells with a slower turnover rate will display late effects

over a period of months to years (Thomas 2006). The risk of late effects to, for example, the spinal cord or lungs, is often a limiting factor to the amount of dose delivered in a radiation therapy treatment (Thomas 2006).

Surgery plays an important role in the treatment of cancer. Though not as necessary today as it once was due to CT, PET, MRI and ultrasound techniques, surgery still plays a role in diagnosis and staging (*e.g.* staging of ovarian cancer, excision biopsy of lymph nodes) (Thomas 2006). When a tumour is locally confined, surgical resection of the diseased tissue is often used as the primary treatment (Thomas 2006). Surgical removal of metastatic lesions involves the resection of tissue that has been invaded by metastases from the primary tumour. Preventative surgery removes tissue or an organ that is at risk of developing cancer, such as bilateral mastectomies in women who carry the BRCA1 and BRCA2 breast cancer genes (Thomas 2006). Reconstructive surgery involves the reconstruction of a removed organ, such as the construction of a false rectum after a panproctocolectomy, to remove the need for a permanent stoma bag. Finally, palliative surgery is performed to help easy patient suffering (Thomas 2006).

Photodynamic therapy (PDT) is a cancer treatment option that allows a higher degree of specificity in targeting malignant and pre-malignant cells than either chemotherapy or radiation, and is less invasive than surgery. The achievement of specificity is a two-fold process: first, photosensitizing drugs are retained preferentially in tumour tissue (Wilson 1986, Chwilkowaka 2003), and second, treatment light of a wavelength that corresponds to an absorption band of

the photosensitizer (PS), is applied selectively to the tumour area, resulting in excitation of the photosensitizer only within that area. The excited photosensitizer subsequently transfers its energy to ground state oxygen, exciting it to its first excited singlet state, and cell death occurs as a result of the damage caused by the singlet oxygen within the cell. Low collateral damage to normal tissue is achieved by applying treatment light only to the tumour (Chwilkowaka 2003). Figure 1-1 shows the photodynamic pathway.

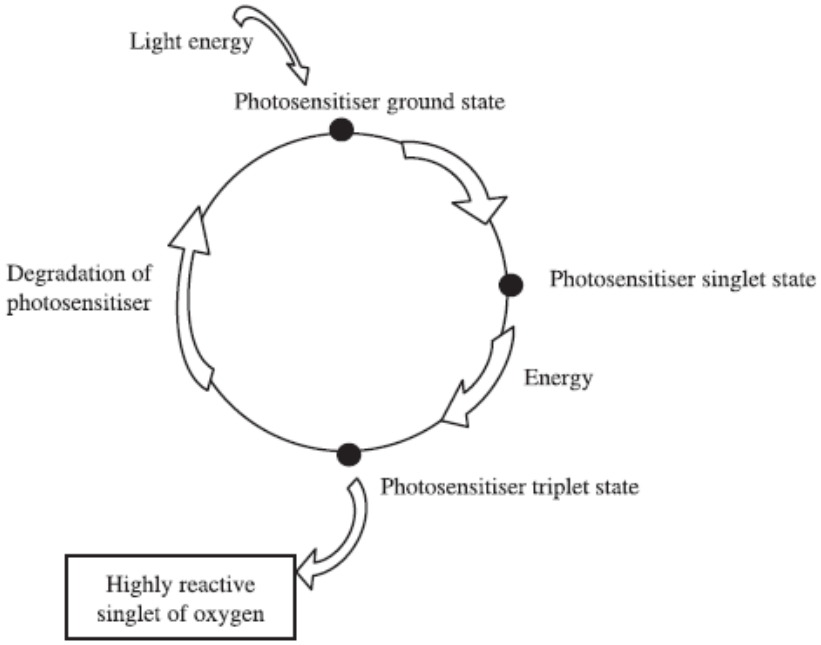

Figure 1-1 The photodynamic therapy pathway: Light energy is introduced to the photosensitizer in its ground state, exciting the molecules to their first excited singlet state. Conversion to the triplet state via intersystem crossing allows the photosensitizer to interact with oxygen in its triplet ground state, resulting in highly reactive singlet oxygen (Claydon 2004)

While the adverse side effects of chemotherapy and radiation therapy impose limits on the number of times a patient can safely undergo these treatments, PDT leaves the healthy tissue surrounding the tumour undamaged, allowing for repeated treatments of the tumour if necessary. PDT may also be

used in adjunct with traditional treatments, such as post surgery PDT to a resection site, for example.

1.2 Two Photosensitizers for Photodynamic Therapy: Photofrin® and delta-Aminolevulinic Acid Induced Protoporphyrin IX

Photofrin® and delta-aminolevulinic acid (ALA) induced protoporphyrin IX (PpIX) are two PDT photosensitizers that have been approved for clinical use. Photofrin® is currently approved for selected oncology applications, such as partially or completely obstructing esophageal cancer, partially or completely obstructing endobronchial cancer, and non-small cell lung cancer (Williams 2004). The current FDA-approved dosage for Photofrin® follows a clinically determined mean dose based on patient body weight of 2 mg/kg delivered intravenously, and 200 to 300 J/cm of excitation light (if delivered by a cylindrical diffusing optical fibre) at 630 nm, depending on the application (US Food and Drug Administration 2007). Photofrin® is typically administered intravenously 48 hours prior to treatment, and often results in patients experiencing photosensitivity (especially in the skin) for up to 3 months after treatment (Claydon 2004). ALA-induced PpIX is, at present, in clinical trials for many applications besides the treatment of the pre-cancerous skin condition actinic keratosis, for which it has already been approved (Bissonette 2004). ALA can be administered topically, or even orally 4 to 6 hours before treatment, with a dose of 30 mg/kg having been shown to result in minimal side effects in trials for

the treatment of Barrett's esophagus, followed by 100-200 J/cm^2 (Claydon 2004). For treatment of actinic keratosis, ALA is applied topically 14-18 hours prior to the administration of 10 J/cm^2 of blue light (Dougherty 2003). It clears rapidly from the body, resulting in local photosensitivity that lasts only 24-48 hours (Claydon 2004).

Photofrin®, or porfimer sodium, consists of monomeric hematoporphyrin, protoporphyrin and monohydroxyethylvinyl-deuteroporphyrin, and oligomeric (dimer to hexamer derivatives of hematoporphyrin units linked through ether or ester bonds) porphyrins, partially purified to contain a reduced fraction of less-photoactive components compared to hematoporphyrin derivative (HpD) (Calzavara-Pinton 2007), with an approximate molecular weight of 600 g/mol. Photofrin® is a lipophilic sensitizer, and as such it is taken up directly through the cell membrane and tends to accumulate in the mitochondrial membrane (Dougherty 1998).

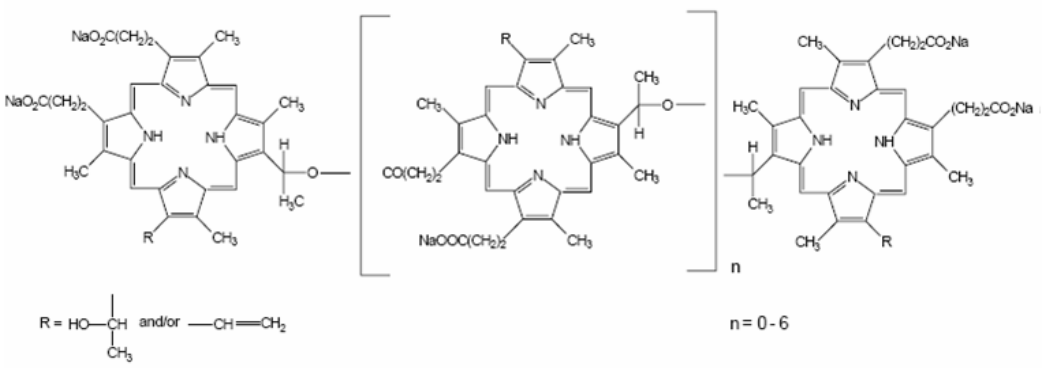

Figure 1-2 The molecular structure of Photofrin® (Axcan Pharma Inc 2005)

The strongest absorption peak for Photofrin® is the Soret band, centered at about 400 nm, with smaller Q-bands found in the green and red, with the weakest

at about 630 nm. Most PDT is performed at wavelengths beyond 600 nm, where absorption by blood and multiple scattering by tissue is reduced, resulting in increased light penetration. Photofrin® is a fluorophore, and as such emits light of a longer wavelength after absorbing light energy. The main fluorescence peak of Photofrin® is centered at 635 nm, with a smaller peak around 700 nm. Photofrin® is also known to degrade into photoproducts which themselves fluoresce, with a peak arising centered at 658 nm (Dysart 2005). Ruck *et al.* have reported fluorescence from aggregates and photoproducts in the 651–663 nm range (Ruck 2007). Figure 1-3 shows the absorption and emission spectra for Photofrin®.

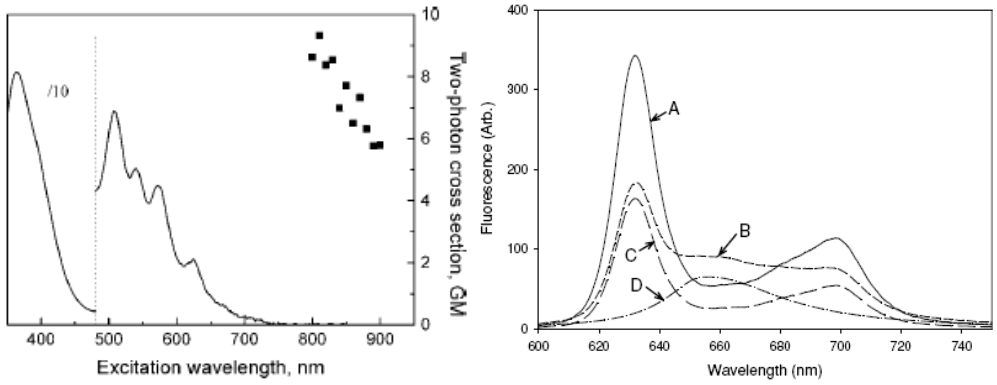

a) b)

Figure 1-3 a) Photofrin® one-photon (solid) and two-photon (data points) absorption spectra (Wilson 2006); b) Emission spectra of Photofrin® before PDT (A), the resulting spectrum after PDT (B) consisting of Photofrin® (C) with photoproduct (D) centered at 658nm (Dysart 2005)

Unlike Photofrin®, PDT with ALA-induced PpIX does not involve direct administration of the photosensitizing agent, since injectable PpIX is not well retained in tissues, including tumours, and clears the body very rapidly (Henderson 2003). Accumulation of PpIX in tissue can, however, be achieved by introducing excess ALA (Dougherty 2003). Both ALA and PpIX are intermediate

molecules in the heme synthesis pathway, shown in Figure 1-4. ALA is administered topically, and once taken up by cells, it is metabolized via the heme biosynthetic pathway to PpIX. ALA is a hydrophilic molecule, and is taken up by active transport into mammalian cells, a process that requires energy and depends on pH and temperature. These systems are slow and saturable, and are slightly more active in tumour cells (Calzavara-Pinton 2007).

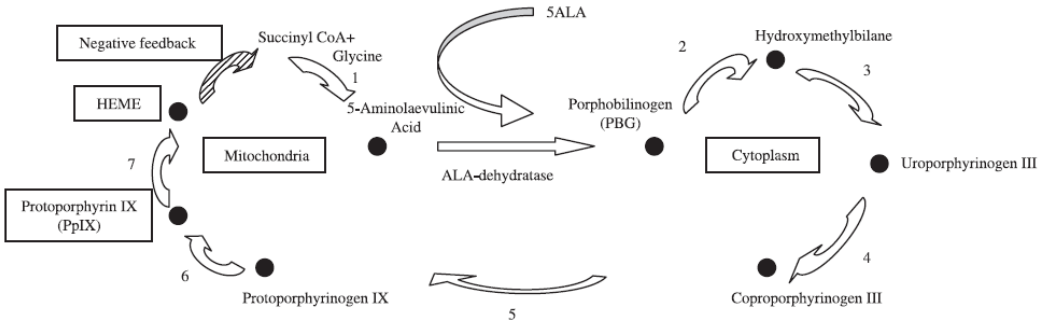

Figure 1-4 The heme synthesis pathway. Addition of exogenous ALA bypasses the negative feedback from the presence of heme, and PpIX is metabolized inside the mitochondria (Claydon 2004)

Negative feedback from the presence of heme inhibits the production of more ALA from glycine and succinyl Co-A by the enzyme delta-aminolevulinic acid-synthetase under normal physiological conditions; this control point is bypassed by adding exogenous ALA. After passing through several intermediates in the cytoplasm, the intermediate coproporphyrinogen III is exposed to coproporphyrinogen oxidase in the mitochondria, forming protoporphyrinogen, which is then metabolized to PpIX, also within the mitochondria. If an excess of PpIX is synthesized, it can diffuse out of the mitochondria and into the endoplasmic reticulum and/or plasma membrane, other sites that are known to

sustain cellular damage during ALA-induced PpIX PDT (Calzavara-Pinton 2007). The rate at which ALA-induced synthesis and accumulation of PpIX proceeds is accelerated in malignant and premalignant tissue compared to normal tissue (Calzavara-Pinton 2007). In Barrett's esophagus, for example, there exists an imbalance between the activity of two enzymes – increased activity of porphobilinogen deaminase, which acts at step 2, and decreased activity of ferrochelatase, which acts at step 7 (see Figure 1-4) – resulting in selective accumulation of PpIX in the tumour as opposed to normal tissue (Claydon 2004, Kondo 1993). In the treatment of Barrett's esophagus, PpIX, unlike other photosensitizers, has been found to accumulate nearly exclusively in the mucosa, as opposed to the submucosa or muscularis mucosa. This limits the treatment depth to around 0.5 mm, which is sufficient to destroy the metaplastic columnar epithelium while restricting tissue damage only to the mucosa, reducing the risk of stricture or perforation (Claydon 2004). PpIX clears the body as it is naturally metabolized to heme.

PpIX exhibits a high absorption peak in the Soret band centered at 405 nm, as well as smaller Q absorption bands, at 510, 545, 580 and 630 nm. Most clinical studies have used light in the 625-633 nm range to excite PpIX for the same reasons as mentioned for Photofrin®. It has been found, however, that treatment with green and blue light demonstrates similar effectiveness for treatment of actinic keratosis while causing less pain than red light (Calzavara-

Pinton 2007). The molecular structure and absorption spectrum of PpIX are shown in Figure 1-5.

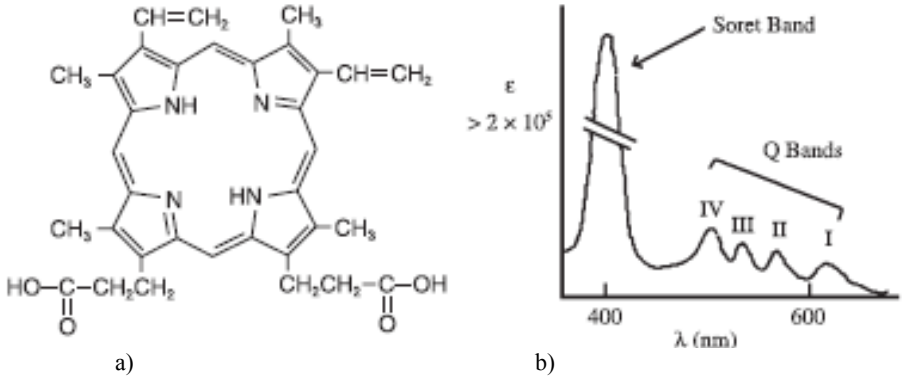

a) b)

Figure 1-5 a) Chemical structure of PpIX; b) Absorption spectrum of PpIX (Calzavara-Pinton 2007)

The main fluorescence peak of PpIX is centered at 635 nm with a smaller peak appearing around 705 nm, with several fluorescent photoproducts at both longer and shorter wavelengths, as seen in Figure 1-6. This study has observed only one photoproduct, photoprotoporphyrin, whose peak is centered at about 675 nm.

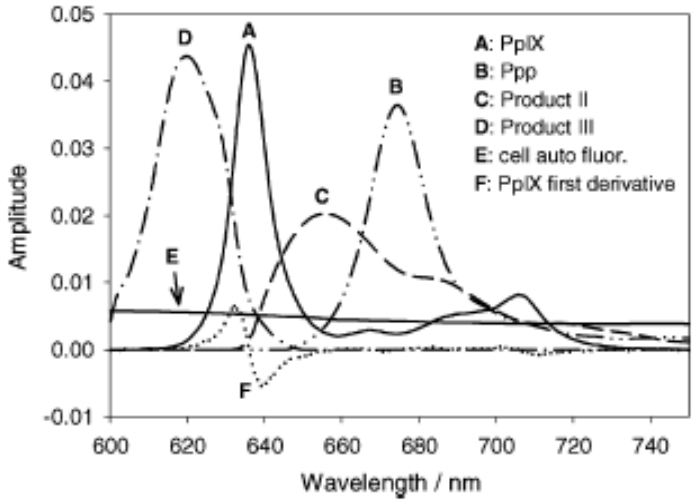

Figure 1-6 The emission spectrum of PpIX (curve A) and its photoproducts (curves B through D) (Dysart 2006)

1.3 Photodynamic Therapy: From Drug Administration to Cell Death

Photodynamic therapy begins with the administration of a photosensitizing agent, introduced either intravenously or topically. Topically applied sensitizers rely on the greater permeability of the abnormal stratum corneum that lies over tumour tissue or inflammatory skin diseases (Dougherty 1998). Lipophilic sensitizers such as Photofrin® are taken up directly through the cell membrane, with penetration increasing with the lipophilicity of the molecule, and tend to localize in the mitochondria. Low tumour pH is one possible reason for the selective uptake of Photofrin®, as the lipophilicity of a molecule increases with decreasing pH (Dougherty 1998). Tumour-associated macrophages have been observed to take up a large amount of HpD and Photofrin®, thus taking part in the selective uptake of sensitizers by tumours (Dougherty 1998). Hydrophilic sensitizers, or precursors such as ALA, are taken up through active transport systems such as pinocytosis (Calzavara-Pinton 2007). PpIX is produced in the mitochondria, as previously discussed, thus it also accumulates there. After a period of hours to tens of hours, preferential drug accumulation in tumour cells is achieved. Sensitizer molecules can exist as monomers or as aggregates; typically, molecules existing as monomers are most able to participate in photochemical reactions.

The laser is the most commonly used light source in PDT. While conventional lamps have also been used, they introduce a thermal component and add difficulty in calculating light dose. Lasers are advantageous as they produce

light that is monochromatic, allowing only light matching an absorption band of the photosensitizer to be delivered and contributing to easier light dosimetry calculations, as well as the ease of incorporating fiber optics for convenient delivery (Claydon 2004).

Once treatment light corresponding to one of the photosensitizer's absorption bands is applied to the treatment volume, the first step in the photochemical processes that constitute PDT is the absorption of a photon by the ground state photosensitizer, promoting it to the short-lived excited singlet state, as seen in the Jablonski diagram, Figure 1-7. The singlet state then decays back to the ground state by collision with another molecule or by emitting a fluorescent photon, or it undergoes intersystem crossing, converting to the metastable triplet excited state, whereby the promoted electron undergoes spin conversion.

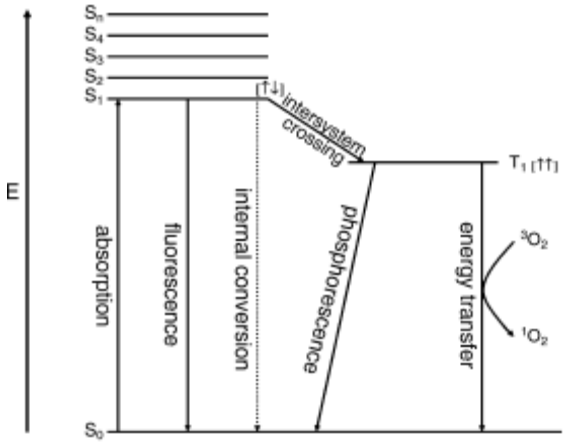

Figure 1-7 Jablonski diagram of the various energy states of excited photosensitizers. S_0 represents the ground singlet state, and S_1 through S_n depict excited singlet states. Note that the S levels are, in actuality, spaced as $1/n^2$. T_1 represents the first excited triplet state. Internal conversion and intersystem crossing are nonradiative transitions, meaning that no photons are released (Calzavara-Pinton 2007)

To understand the difference between the singlet and triplet states, it is instructive to make note of spin multiplicity. The spin multiplicity of an electronic state is given by M = 2S + 1, where S is the angular momentum quantum number. When all electrons in a molecule are configured such that their spins are paired (*i.e.*, each electron pair consists of an electron with an upward spin and an electron with a downward spin), the angular momentum is 0 and M is equal to 1; this is the singlet state, and the ground state for most molecules. Consider a photosensitizer in the excited singlet state: if that excited electron were to undergo a spin conversion, the result would be two unpaired electron spins (either both upward or both downward) and the net angular momentum would be 1, yielding a multiplicity of 3; the photosensitizer would then be in a triplet state. The triplet state is metastable for most molecules; however it survives long enough to take part in chemical reactions (Calzavara-Pinton 2007).

At this point, one of two reactions may occur. In a type I photoprocess, an electron or a proton is transferred between the triplet state photosensitizer and other nearby molecules, resulting in the production of reactive oxygen species that are harmful to cells, such as superoxides, hydroperoxyls, hydroxyl radicals, and hydrogen peroxide, returning the PS to the ground state (Calzavara-Pinton 2007). In a type II photoprocess, an electron spin exchange occurs between the triplet state PS and molecular oxygen ($^3O_2$), which is unusual in that its ground state is the triplet state. This produces cytotoxic excited singlet oxygen ($^1O_2$), and the photosensitizer returns to ground state (Calzavara-Pinton 2007). Both type I and

type II photoprocesses result in oxidation of biomolecules, however singlet oxygen is considered to be the main cytotoxic agent in PDT (Calzavara-Pinton 2007). A summary of these processes is shown in Figure 1-8.

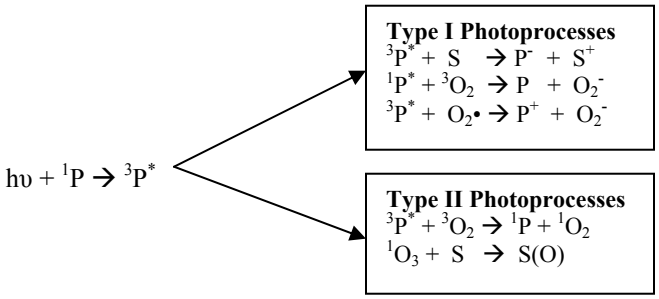

Figure 1-8 Summary of type I and type II photoprocesses that occur following photosensitizer excitation and conversion to the triplet state. ^1P represents the photosensitizer in the singlet ground state, and $^3P^*$ denotes the photosensitizer in the triplet excited state. S denotes a substrate molecule. A superscripted '+' indicates an oxidized molecule while a superscript '-' indicates a reduced molecule. $^3O_2$ is molecular oxygen in its triplet ground state, O_2^- is the superoxide anion, $O_2\bullet$ is the superoxide radical, $^1O_2$ is oxygen in its singlet excited state, and S(O) denotes oxygen with adduct of substrate. (figure adapted from Henderson 2003)

The localization of the photosensitizer determines the type of damage that will occur, since singlet oxygen, the principle PDT cytotoxic agent, can only diffuse up to 0.02 μm during its <0.04 ms lifetime (Calzavara-Pinton 2007, Peng 1998). Reactive oxygen species such as singlet oxygen are powerful oxidants that react with many different kinds of biomolecules, including unsaturated triacyl glycerols, cholesterol, phospholipids, some amino acids, and some nucleic acid bases (Calzavara-Pinton 2007). Singlet oxygen can react with biomolecules in several ways, including the 'ene' reaction, which involves a hydrogen abstraction and oxygen addition (Dougherty 1998). This reaction degrades plasma membranes by lipid peroxidation (Claydon 2004, Peng 1998). Singlet oxygen

therefore acts as an oxidizing intermediate, initiating a chain reaction in which lipid radicals are produced. Alterations to the membrane lipids and membrane proteins take the form of lipid-lipid, lipid-protein or protein-protein cross-links, compromising membrane integrity (Dougherty 1998).

While the molecular and signaling mechanisms of apoptotic cell death are for the most part unknown, it is known that the ability of a photosensitizer to trigger apoptosis is greatest for those sensitizers that localize in the mitochondria. This is because the mitochondria have key functions in apoptotic regulation (Calzavara-Pinton 2007). Upon irradiation, ATP production in the mitochondria is inhibited, and damage is sustained to respiratory chain complexes III, IV and I, followed by the rapid release of mitochondrial cytochrome *c*, a trigger of apoptotic response. Cytochrome *c* release is known to precede the activation of caspases, leading to the irreversible cleavage of certain cellular proteins that exhibit structural, signaling or transcriptional functions (Calzavara-Pinton 2007).

Aggregates are taken up by pinocytosis, and thus become localized in lysosomes or endosomes. Light exposure causes the lysosomes to become permeable, releasing hydrolytic enzymes into the cytoplasm (Dougherty 1998). Sensitizers that localize in the plasma membrane tend to lead to necrosis once treatment light is applied (Dougherty 1998). Most photosensitizers used for PDT do not accumulate in the nucleus, thus there is a low potential for PDT to give rise to DNA damage, mutations or carcinogenesis (Dougherty 1998). The

photodynamic pathway from drug administration to cell death is summarized at the end of this chapter.

Additionally, hydrophilic sensitizers can localize preferentially in newly formed vessels of tumour and inflammatory tissues. These newly formed vessels exhibit greater permeability and poor lymphatic drainage, which aids uptake and retention of sensitizers in these tissues. Reactive oxygen species damage endothelial cells, disrupting their barrier function, causing loss of tight junctions and exposing the vascular basement membrane. This leads to activation of platelets, leucocytes and the release of proaggregatory agents. The result is constricting arterioles, thrombotic occlusion of venules, and blood stasis which results in hypoxia and nutrient deprivation (Calzavara-Pinton 2007). This damage can also serve to diminish the oxygen supply to the tumour during PDT, however vasculature damage occurring post-PDT contributes to long-term tumour control (Dougherty 1998).

Total tumour eradication, however, is challenging. One limitation may be the inhomogeneous distribution of the sensitizer in the tumour as well as hypoxia induced by the increasing distance of tumour cells from vasculature (Dougherty 1998). Since singlet oxygen is generated from ground state oxygen, PDT treatment tends to rapidly consume oxygen in the tissue, creating additional regions of hypoxia where PDT is less effective. Rates of singlet oxygen generation, and therefore tissue oxygen depletion, are high for high concentrations of photosensitizer and high fluence rates. The fluence rate can be lowered to slow

the consumption of oxygen and thereby maintain oxygen levels in the tissue during treatment. Photobleaching also influences the rate of tissue oxygen consumption, as reduction in sensitizer concentration also reduces the rate of consumption (Dougherty 1998). Fractionation of light delivery is another means by which to control tissue oxygen levels, by allowing for reoxygenation of the treatment site. Administering short light and dark intervals, on the order of 20 – 50 s is sufficient for reoxygenation during the dark intervals (Dougherty 1998).

1.4 The Need for Dosimetry in Photodynamic Therapy and Current Non-Lifetime Based Methods

The efficacy of PDT is dependent on the concentration of the photosensitizer in the tissue to be treated, and is therefore most effective when proper dosing is achieved. Drug accumulation, light absorption, and levels of oxygenation, however, differ from patient to patient and between different sites in the same patient (Wilson 1986). These differences in photosensitizer uptake levels, oxygenation, and light absorption often lead to over- or underdosing. Overdose may cause damage to the surrounding normal tissue while underdose may result in residual dysplasia or malignant tissue. Current dosing guidelines, however, are not patient-specific and are defined by empirical values. The local tissue concentration of the photosensitizer is not easily controlled, but the amount of treatment light applied to the affected area can be adjusted. Knowledge of the local tissue concentration of photosensitizer would allow light doses to be tailored

to compensate for the variable amounts of photosensitizer. In order to help regulate dosing, then, real-time methods to monitor the photosensitizer concentration in the target tissue (Wilson 1986), and its interactions with elements of the cellular environment are of great practical importance.

Fluorophore concentration in tissue can be determined by drawing blood or performing biopsies followed by analysis, such as chemical extraction (Diamond 2005), but these techniques are invasive and do not give real-time results. Chemical extraction takes 4 – 12 hours, during which time the tissue sample is digested in 0.1 N sodium hydroxide before centrifuging and measuring the fluorescence from the supernatant and comparing it with a known standard (Diamond 2004). Due to the rapid clearance rate of many sensitizers, however, this method would not provide timely or accurate dosimetry for treatment. It is important to know the drug concentration in the target tissue at the time of treatment, so that the proper light dose can be administered. Less invasive, real-time optically-based methods for determining photosensitizer concentration have been based on fluorescence, absorption, and reflectance spectroscopy. The measured fluorescence signal is proportional to the product of the fluorophore concentration and fluorescence quantum yield, and depends on optical properties of the tissue, the local microenvironment, and geometry of excitation and detection (Potter and Mang 1984, Canpolat and Mourant 2000a). Measured fluorescence is compared to a model, or a calibration curve derived from chemical

extraction measurements performed on similar tissues in order to derive a concentration (Panjehpour 1993).

Measurements of aluminum phthalocyanine tetrasulfonate ($AlPcS_4$) concentration in rabbits were performed by Weersink *et al.* by using *in vivo* reflectance spectroscopy, observing the fluorescence and reflectance of excitation light at two different source-detector separations, and comparing measurements to a calibration performed in tissue-simulating phantoms (Weersink 2001). Accurate concentration estimates were found for measurements made in the liver; however those made in the skin were affected by its multilayered structure.

Measurements based on changes in absorption (elastic scattering spectroscopy, ESS) were performed in an animal tumour model by Mourant *et al.* to quantify the tissue concentration of two chemotherapy drugs, Doxorubicin and Mitoxantrone, using a single optical fibre source-detector pair, with the separation between the fibres chosen to minimize the influence of tissue scattering properties (Mourant and Bigio 1999). Though the measured concentrations were linear with the concentrations determined by chemical extraction, they yielded concentration estimations that were consistently below those determined by extraction.

Panjehpour *et al.* measured sulphonated aluminum phthalocyanine fluorescence in rats, and determined that the fluorescence depended linearly on concentration, as measured by chemical extraction (Panjehpour 1993). Lee *et al.* measured $AlPcS_2$ concentration *in vivo* in muscle and liver using a fibre bundle probe and compared the results to chemical extraction (Lee 2001). It was found

that differences in the fluorescence quantum yield and in the partition of photosensitizer between blood and tissue, as well as absorption of the excitation light by hemoglobin, led to some discrepancies between the results in muscle.

Steady-state imaging faces certain complications when measuring fluorescence. Both the fluorophore's extinction coefficient spectrum and the fluorescence quantum yield may be influenced by the local environment, which would result in an inaccurate estimation of concentration if the estimate were based solely on the amplitude of the fluorescence signal (Diamond 2004). For these reasons, steady-state spectral imaging provides information regarding drug localization (Diamond 2003), but is not a quantitative measure of local drug concentration. Interference from cellular autofluorescence and absorption by various chromophores, the most significant of which are hemoglobin and melanin in tissue, are also obstacles. These problems may be circumvented by the addition of fluorescence lifetime information, which is unaffected by the above mentioned sources given sufficient signal-to-noise ratio. In addition, changes in the fluorescence lifetime of a photosensitizer can yield much information about the drug's interactions with the cellular environment, such as oxygen and the tissue microenvironment (Schaferling 2005, Diamond 2005). Time-resolved fluorescence has been applied to macroscopic applications in chemical imaging (Lakowicz 1999), investigation of atherosclerosis (Tang 2000), and diagnostics of tumours (Richards-Kortum 1996, Torricelli 2001, Pitts, 2001). These studies suggest that the use of lifetime information not only improves the specificity of

fluorescence-based techniques, but also allows a more robust evaluation of *in vivo* data.

1.5 The Meaning of Fluorescence Lifetime, and Fluorescence Lifetime Based Methods for Dosimetry in Photodynamic Therapy

The fluorescence emission of a fluorophore follows an exponential decay, single or multiple, defined by the average lifetime that the fluorophore remains in the excited state. This property is the fluorescence lifetime. Once excited by a pulse of light, the fluorophore will deexcite via both radiative and nonradiative processes at a rate which depends on both the radiative or emissive rate of decay (Γ) and the nonradiative rate of decay (k_{nr}),

$$\frac{dn(t)}{dt} = (\Gamma + k_{nr})n(t) \qquad (1.1)$$

where n(t) gives the number of fluorophores in the excited state at a time t after the initial excitation (Lakowicz 1999). The total decay rate is the sum of the radiative and nonradiative decay rates, and the lifetime, τ, is given by the inverse of the total decay rate (Lakowicz 1999)

$$\tau = \frac{1}{\Gamma + \mathrm{k_{nr}}} \qquad (1.2)$$

The exponential decay of the population in the excited state is then determined by integrating equation 1.1

$$n(t) = n_0 e^{\frac{-t}{\tau}} \qquad (1.3)$$

Note that we observe the time-dependent intensity of the emitted fluorescence, as opposed to the number of molecules in the excited state, so equation 1.3 can be re-written in terms of intensity to obtain the expression for a monoexponential fluorescence decay (Lakowicz 1999)

$$I(t) = I_0 e^{\frac{-t}{\tau}} \tag{1.4}$$

The fluorescence quantum yield is the number of photons emitted relative to the number of photons absorbed (Lakowicz 1999), and reflects the competition between the radiative and nonradiative decay rates (Lakowicz 1999). The fluorescence quantum yield (Φ) is given by the radiative decay rate over the total decay rate

$$\Phi = \frac{\Gamma}{\Gamma + k_{nr}} = \frac{\tau}{\tau_n} \tag{1.5}$$

The natural fluorescence lifetime, τ_n, is considered to occur in the absence of nonradiative processes, and is thus the inverse of the radiative decay rate (Lakowicz 1999).

Diamond *et al.* explored two fluorescence-based techniques to measure the concentration of $AlPcS_4$ in tissue, and compared results to *post mortem* chemical extraction and fluorometric assay (Diamond 2005). The first technique was a steady-state method used by Weersink *et al.* that depends on the ratio between fluorescence and scattered excitation light as collected at two different source-detector separations (Weersink 2001). The second method was based on time-resolved measurements of the fluorescence lifetime. A single optical fibre was

used for both excitation and fluorescence detection (Diamond 2005). For each technique, a line of best fit of measured signal *versus* concentration as determined in the calibration phantoms was used for estimates of photosensitizer concentration in tissue. The area under the curve of the fluorescence decay obtained by measuring the time-resolved fluorescence was used as the total fluorescence signal for the concentration curve, where the fluorescence decay was estimated using a weighted least-squares fit to a single exponential decay (Diamond 2005). While Vishwanath *et al.* (Vishwanath 2002) found that fluorescence lifetime did not depend on the optical properties of the tissue simulating phantom, Diamond *et al.* found that there was a slight dependence in their interstitial measurements, likely owing to an increase in the mean length of the path that the fluorescence traveled before detection (Diamond 2005). In the calibration phantom, Diamond *et al.* found that the influence of differences in optical properties between surface and interstitial measurements yielded differences in fluorescence lifetime of 0.3 ns. Both the steady-state and the fluorescence lifetime technique yielded similar results *in vivo* for low concentrations. Both techniques agreed well with values determined by chemical extraction at low concentrations, especially for skin, muscle and fascia, however underestimated concentration at higher doses, especially in liver and kidney tissues, though the single fibre fluorescence lifetime method yielded more accuracy in these cases (Diamond 2005).

Since molecular binding is one of the factors that influences fluorescence lifetime, it is necessary to characterize the lifetime of the photosensitizers when localized in cells. This can be achieved using fluorescence lifetime imaging microscopy (FLIM), which provides spatially resolved lifetime information. Over the past decade, several FLIM techniques have been developed including frequency domain modulation (Lakowicz 1999), time-domain scanning using a gated intensifier (Cubeddu 2002, Dowling 1998, Siegal 2001, Vishwanath 2004, Periasamy 1996, Chen 2004), one-dimensional spatial scanning with a streak camera (Glanzmann 1999), and 3-D raster scanning in space through time-correlated single photon counting (TCSPC) (Egner 2000). So far, FLIM applications are primarily limited to *in vitro* cellular studies with only a few exceptions (Torricelli 2001, Elson 2002). *In vivo* fluorescence lifetime characterization has applications for future PDT monitoring, as observing changes in the fluorescence lifetime may yield information regarding the photosensitizer's interaction with the cellular environment, as well as dosimetry.

The objective of this work was to quantitatively characterize fluorescence lifetime of Photofrin® and ALA-induced PpIX localized in living cells using a TCSPC based FLIM system. The fluorescence lifetime of both photosensitizers in solutions at physiologically-relevant concentrations were also measured under single and two-photon excitations as references. These data will serve as a baseline for future studies at the tissue level using time-domain spectroscopy and imaging technologies for real-time PDT dosimetry.

The Photodynamic Therapy Pathway

Drug Administration

- Intravenously or topically
- Dosages currently based on clinically determined means

Drug Accumulation

- Takes hours to tens of hours

Hydrophobic (Lipophilic) Sensitizers/Precursors
- ex. Photofrin®
- taken up directly through cell membranes
- lipophilicity increases with pH; low tumour pH facilitates preferential accumulation
- tumour-associated macrophages participate in selective uptake
- tend to accumulate in mitochondria

Hydrophilic (Lipophobic) Sensitizers/Precursors
- ex. ALA
- taken up by active transport
- energy is required, and depends on pH and temperature
- active transport systems are slow and saturable, and slightly more active in malignant cells

- aggregates are taken up by pinocytosis and localize in lysosomes or endosomes

Photosensitizer Accumulation

applicable only to sensitizers introduced via their metabolic precursors

- ex. ALA-induced PpIX (intermediates of the heme synthesis pathway)
- introduction of exogenous ALA bypasses negative feedback from the presence of heme, which regulates the synthesis of endogenous ALA
- synthesis passes through several intermediates in cytoplasm
- coproporphyrinogen oxidase acts on coproporphyrinogen III in the mitochondria, forming protoporphyrinogen, which is metabolized to PpIX, also in the mitochondria
- increased activity of enzymes porphobilinogen deaminase at step 2, and decreased activity of ferrochelatase at step 7 in tumor cells results in selective accumulation of PpIX

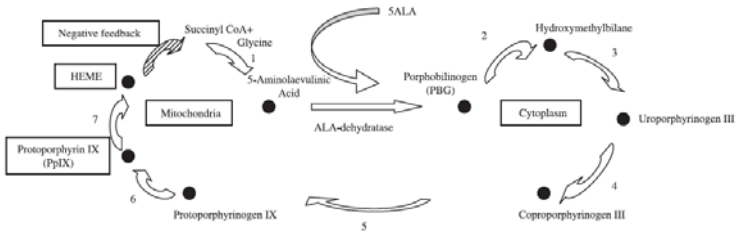

Application of Treatment Light

- monochromatic laser light corresponding to an absorptive region of the photosensitizer to minimize thermal component
- delivery can be aided by fiber optics

Photosensitizer Excitation and Conversion to the Triplet State

- absorption of a photon of light by ground state photosensitizer molecules promotes them to the short-lived excited singlet state
- may decay back to ground state radiatively (by emitting a fluorescent photon) or non-radiatively (by internal conversion) *or*
- may undergo intersystem crossing, converting to the triplet excited state, whereby the promoted electron undergoes a spin conversion
- the triplet state is sufficiently long-lived to take part in chemical reactions

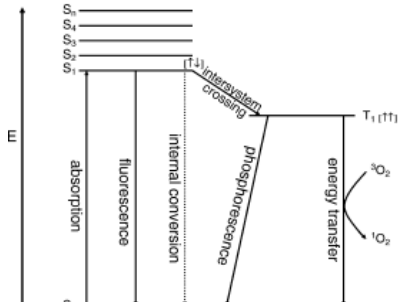

Generation of Reactive Oxygen Species

- excited photosensitizer molecules in the triplet state react with nearby molecules, including oxygen via either type I or type II photoprocesses
- the generation of singlet oxygen by a type II photoprocess is most significant, as singlet oxygen is the main PDT-induced cytotoxic agent

Type I

$^3P^* + S \rightarrow P^- + S^+$

$^1P^* + {}^3O_2 \rightarrow P + O_2^-$

$^3P^* + O_2\bullet \rightarrow P^+ + O_2^-$

Type II

$^3P^* + {}^3O_2 \rightarrow {}^1P + {}^1O_2$

$^1O_3 + S \rightarrow S(O)$

Damage Caused by Singlet Oxygen

- reacts with many different kinds of biomolecules (unsaturated triacyl glycerols, cholesterol, phospholipids, some amino acids, and some nucleic acid bases) via the 'ene' reaction (a hydrogen abstraction and oxygen addition)
- plasma membrane degradation is caused by singlet oxygen performing lipid peroxidation by the 'ene' reaction
- singlet oxygen acts thus initiates a chain reaction in which lipid radicals are formed
- membrane lipids and membrane proteins are altered as lipid-lipid, lipid-protein and protein-protein crosslinks form from the radicals
- membrane integrity is compromised

Cell Death

Sensitizers that localize in the mitochondria

- damage to mitochondrial membrane leads to inhibited ATP production and damage to respiratory chain complexes, followed by rapid release of cytochrome c
- cytochrome *c* release precedes the activation of caspases, which irreversibly cleave certain cellular proteins with structural, signaling or transcriptional functions
- apoptosis is induced

Aggregates localized in lysosomes

- damage to lysosomal membrane renders it permeable, and hydrolytic enzymes are released into cytoplasm
- necrosis results

Chapter II – Lifetime Measurements in Organic Solutions using Time Domain (Time-Correlated Single Photon Counting) and Frequency Domain Methods

In order to acquire a baseline indication of fluorescence lifetime for these two photosensitizers, and to validate the technique intended to be used to analyze them in cells, measurements were first made in organic solutions. Measurements using time correlated single photon counting were made first, followed by single-photon measurements made using a frequency domain system for purposes of comparison. Both one- and two-photon excitation were used for measurements made with a streak camera, to investigate the influence of the excitation mode on the lifetime, and also to provide another point of comparison for the lifetimes measured using TCSPC. Measurements were also made of Photofrin® in solution using the FLIM system to validate the use of that instrument; those results will be discussed in Chapter 3, along with the investigations into fluorescence lifetimes in cell cultures that followed the solution based experiments.

2.1 Principles of Time Correlated Single Photon Counting

Time Correlated Single Photon Counting (TCSPC) is a photon collection method used to measure waveforms, and is used in time domain methods to measure fluorescence decays. A sample is repeatedly excited with narrow pulses of light with a certain repetition rate, and after each pulse, a maximum of one fluorescent photon is collected. Repetitive measurements of the detection time

relative to the excitation pulse allow a histogram to be built up that represents the waveform under observation. This process is demonstrated in Figure 2-1.

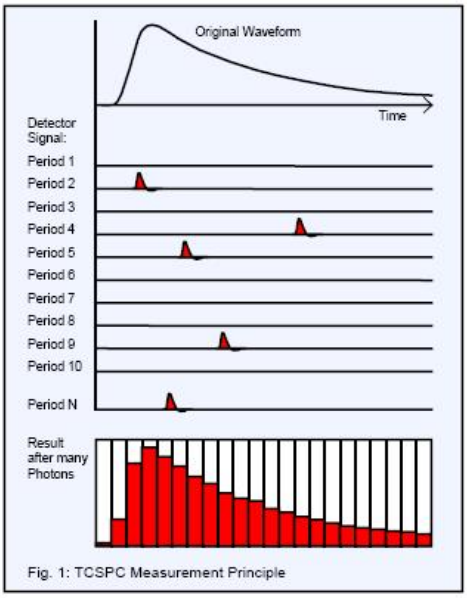

Figure 2-1 After each excitation, zero or one fluorescent photon is detected. Since the intensity of the fluorescence is low, the probability of detecting more than one photon per period is negligible. When a photon is detected, a count is added to the corresponding time channel. After many pulses, the histogram of detection times builds up and the decay can be reconstructed. (Becker 2005)

The excitation source for a TCSPC system should deliver pulses that are narrow enough to be considered delta functions, with a FWHM on the order of picoseconds. For fluorescence decay measurements, the pulse repetition rate should ideally be about four times longer than the expected fluorescence lifetime (Lakowicz 1999) to avoid overlap of consecutive decays. Emitted fluorescence is collected by a photomultiplier tube (PMT). Subnanosecond instrument responses can be obtained because the rising edge of a pulse resulting from the capture of a single photon is quite steep.

Pulses emitted from the PMT will have different amplitudes, and if simple leading edge discrimination were used, they would cross the threshold value at different times, leading to a spread of Δt in pulse detection times, as shown in Figure 2-2a. This is undesirable, as accuracy in timing and detection is very important to retrieving accurate fluorescence lifetimes.

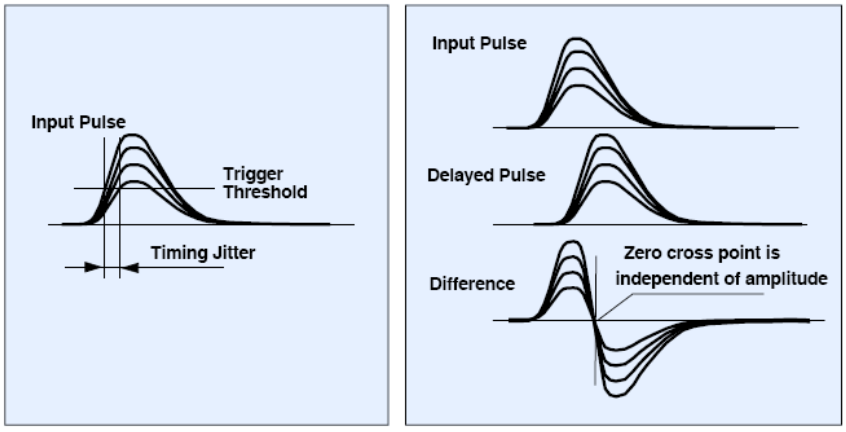

a) b)

Figure 2-2 Leading edge triggering; the threshold is reached at different times, depending on the pulse height, which leads to timing jitter; b) Constant-fraction triggering; the introduction of a zero cross point removes timing jitter due to different pulse heights (Becker 2005)

A constant fraction discriminator (CFD) is used to alleviate this time variation. The CFD contains both a leading edge discriminator and a zero cross discriminator, as shown in the Figure 2-3. The zero cross discriminator splits the signal, then delays and inverts the remainder. Upon recombination, the signal takes on the form shown in Figure 2-2b, exhibiting a zero cross point that is independent of amplitude and can be triggered on by subsequent electronic components to avoid time variations based on pulse height. Since the zero cross discriminator will trigger on signals that are very small, a threshold is established by a leading edge discriminator that it is connected to in parallel. If the incoming

signal crosses the threshold of the leading edge discriminator, the output of the zero cross discriminator is enabled.

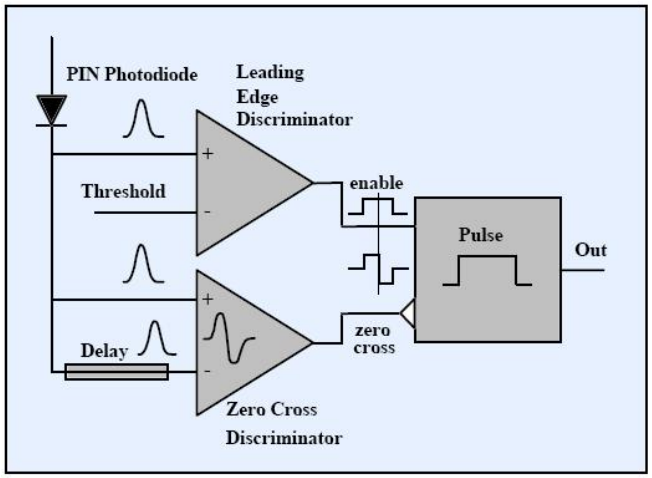

Figure 2-3 Constant fraction discriminator; the zero cross discriminator introduces a zero cross point to eliminate timing jitter due to pulse height, and the leading edge discriminator enables the output from the zero cross discriminator only if the threshold is reached (Becker 2005)

A time-to-amplitude converter (TAC) triggers on the zero cross point of the signal outputted by the CFD. The signal resulting from a detected fluorescent photon constitutes a start pulse, and triggers the TAC to begin charging a capacitor. The stop pulse comes from the next excitation synchronization pulse, and triggers the TAC to stop charging the capacitor, as seen in Figure 2-4.

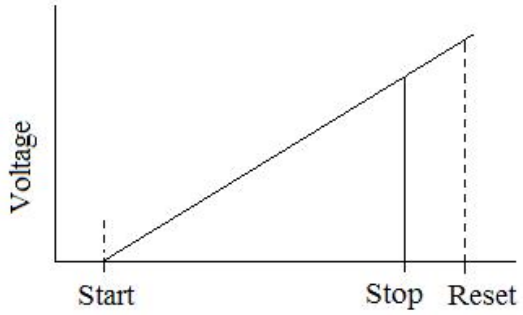

Figure 2-4 Voltage stored in capacitor. The detection of a fluorescent photon triggers the capacitor to begin charging, and the next excitation pulse provides the signal to stop charging; this operation is termed 'reverse mode'.

This operation scheme is referred to as reverse mode, and it is operated in this mode for two reasons. First, it takes several microseconds to discharge the capacitor and reset the TAC. Since there isn't always a fluorescent photon detected, it is inefficient to charge the capacitor if no event occurs during that period. Second, and more importantly, the excitation pulses are occurring on the order of nanoseconds while the TAC requires microseconds to reset – in forward mode, the TAC would be overloaded with continual start pulses. Figure 2-5 demonstrates the detection time measuring scheme for reverse mode. The voltage stored in the capacitor is then proportional to the photon detection time relative to the next laser excitation pulse, and that voltage is outputted to a multichannel analyzer (MCA), which uses an analog-to-digital converter (ADC) to convert the voltage to a time channel. One count is added to the time channel that corresponds to the incoming voltage, and in this manner, the probability histogram is accumulated. Since the TAC is operated in reverse mode, the histogram is constructed backwards and must be reversed to represent the actual time delays.

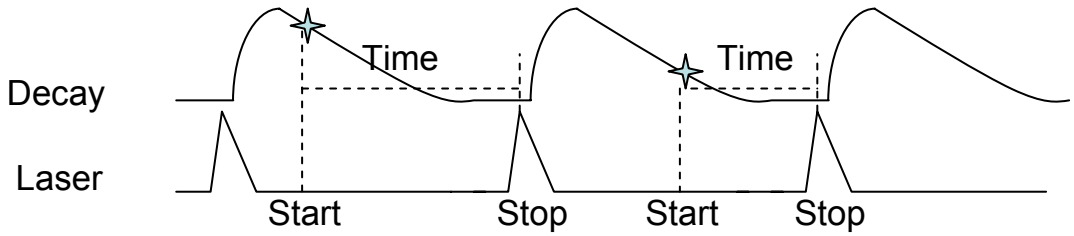

Figure 2-5 Measurement of detection times with the TAC operating in reverse mode; detection times are measured between the detection of a fluorescent photon and the arrival of the next excitation pulse. (diagram by lab summer student Paul Quevedo)

2.2 Principles of Frequency Domain Methods

The frequency domain, or phase-modulation, method for detecting fluorescence lifetimes relies on exciting the sample with light that is intensity-modulated (such as a sine wave, for example). Direct modulation of the laser or down beam electro-optic modulation are often used to accomplish this task. The modulation frequencies are high, usually around 100MHz, so that the reciprocal is comparable to the lifetime (Lakowicz 1999). The fluorescence emission of a fluorophore thus excited responds with the same frequency, however the time spent in the excited state causes the emission to be delayed in time, as shown in Figure 2-6. This phase shift (ϕ) can be used to calculate the phase lifetime (Lakowicz 1999),

$$\phi = \arctan(\omega\tau_\phi) \tag{2.1}$$

Therefore,

$$\tau_\phi = \frac{\tan\phi}{\omega} \tag{2.2}$$

Where ω is the modulation frequency given in radians per second. The fluorescence lifetime also causes a decrease in the peak-to-peak intensity of the emitted signal relative to the excitation signal, an effect called demodulation (Lakowicz 1999). The modulation lifetime can be calculated using this property,

$$m = \frac{1}{\sqrt{1+(\omega\tau_m)^2}} \tag{2.3}$$

Therefore,

$$\tau_m = \frac{1}{\omega}\sqrt{\frac{1}{m^2} - 1} \qquad (2.4)$$

where m is the modulation, as defined in Figure 2-6.

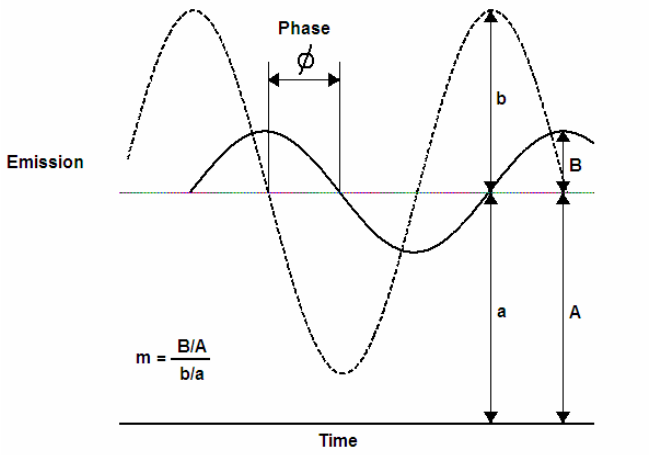

Figure 2-6 Overview of frequency domain lifetime measurements. The dashed curve represents the excitation, and the solid curve represents the delayed fluorescence emission. The modulation is given by 'm', where 'A' and 'a' give the amplitudes of the DC components of the fluorescence and the excitation, respectively, while 'B' and 'b' give half the amplitudes of the modulated fluorescence and excitation signals (figure adapted from Lakowicz 1999).

The phase shift and the modulation both depend on the fluorophore's lifetime and the frequency of the modulation, such that as the frequency increases the phase shift increases and the modulation depth decreases (Lakowicz 1999). For a single exponential decay, equations 2.2 and 2.4 both give the fluorescence lifetime of the fluorophore for a given frequency. For multiexponential decays, they yield apparent lifetimes, each representing a different weighted average of the components of the fluorophore's decay, and nonlinear least-squares analysis is used to recover decay times by fitting to equations 2.1 and 2.3 (Lakowicz 1999). These equations give the frequency response, obtained by measuring the phase shift and modulation over a wide range of modulation frequencies. The shape of

the frequency response is determined by the number of decays present (Lakowicz 1999). As the modulation frequency is increased, the phase shift increases from 0º to 90 º and the modulation decreases from 1 to 0. The homodyne technique, in which high frequency signals are transformed to DC signals, is commonly used to measure the phase shift and modulation (Cubeddu 2002).

2.3 TCSPC Spectroscopy

A schematic of the TCSPC system used for experiments involving Photofrin® and PpIX dissolved in organic solvents is shown in Figure 2-7. The excitation source was a 405 nm picosecond pulsed laser (60ps FWHM, PLP-01, PicoQuant, Berlin, Germany) operated at 20 MHz that was lens-coupled to the cuvette holder. Emitted fluorescence was collected by a lens-coupled fibre on another face of the cuvette, which was oriented at 90º to the excitation light to minimize collection of excitation light. The light signal was passed through a 580 nm longpass filter (Oriel, Stratford, CT) to remove side-scattered excitation light before being collected by a PMT (H5783P-01, Hamamatsu, Hamamatsu City, Japan). The electrical signal from the PMT was then amplified by a 26dB amplifier (HFAC, Becker & Hickl GmbH, Berlin, Germany) and passed through a passive delay generator (TC412A, Tennelec, Lenoir City, TN, USA).

Data were acquired using the SPC-630 TCSPC system (SPC-630, Becker & Hickl GmbH). The SPC-630 setup consisted of a constant fraction discriminator (CFD) followed by a time-to-amplitude converter (TAC). The

multichannel analyzer displayed a histogram of fluorescent photon detection times based on the amplitude of the voltages outputted by the TAC, as previously discussed. Decay constants were fitted using the Marquardt-Levenberg algorithm (Diamond 2005). An instrument response function (IRF) was measured by aligning the source and detection fibres (oriented at 180º through the cuvette holder). A time resolution of 200 ps was determined by measuring the full width at half maximum (FWHM) of the IRF.

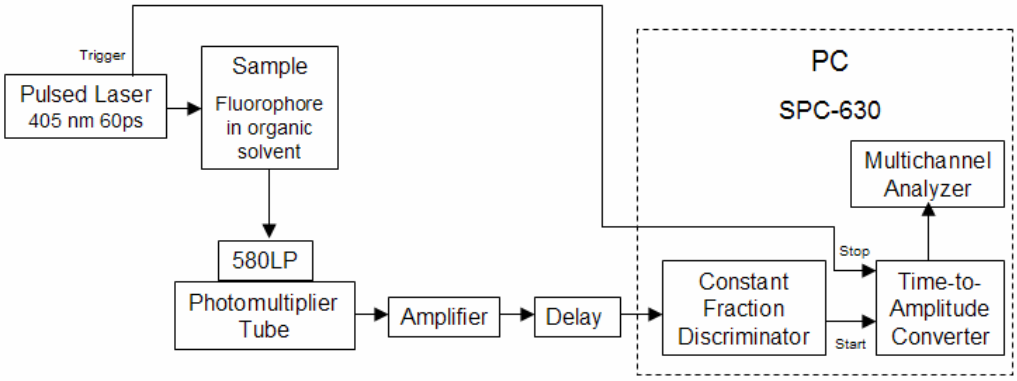

Figure 2-7 Time-correlated single photon counting (TCSPC) schematic.

2.4 Frequency Domain Spectroscopy

The frequency domain system used in this study was the Chronos lifetime spectrometer system (ISS, Champaign, Il). This instrument is designed to accommodate various excitation sources including light emitting diodes (LEDs), continuous wave lasers and mode-locked lasers. Its two frequency generators are capable of providing modulation over a range of 9 kHz up to 1.2 GHz. For samples with fluorescence lifetimes on the order of milliseconds to microseconds, low frequency modulation is available covering a range from 90 Hz up to 1.5

MHz (Terpetschnig 2008). The first synthesizer was used to modulate the light source while the second modulated the gain of the PMT (R928, Hamamatsu). The Vinci multidimensional fluorescence spectroscopy software (ISS) was used to control the Chronos system, as well as all data acquisition and analysis. Vinci uses non-linear least squares methods to determine how closely a user-selected model (such as a monoexponential decay) matches the acquired data, employing a Marquardt-Levenberg algorithm to minimize the χ^2 function for this comparison, and returns the calculated fluorescence lifetime (Terpetschnig 2008). Vinci is capable of fitting multiple decay times, exponential and non-exponential (Terpetschnig 2008).

2.5 Streak Camera Spectroscopy

Measurements of Photofrin® were also performed using a streak camera system (Streak Scope C4334, Hamamatsu, Hamamatsu City, Japan) to examine whether the method of excitation used for the FLIM experiments (two-photon excitation) may affect the measured fluorescence lifetime and yield different results than under single-photon excitation, which is the excitation mode that would be used in clinical PDT dosimetry.

The schematic of the set up is shown in Figure 2-8. Measurements were made under both single-photon excitation around 400 nm, as well as two-photon excitation at 800 nm. Excitation at 800 nm was achieved using a Ti: Sapphire laser (Tsunami, Spectral Physics, Mountain View, CA), pulsed at 80 MHz and

with an output power of 500 mW. Excitation at 400 nm was obtained by frequency doubling using a BBO (β-BaB_2O_4) crystal and a band-pass filter (BG39, Schott, Mainz, Germany) to block the 800 nm light. The average output power at 400 nm was 0.015 mW.

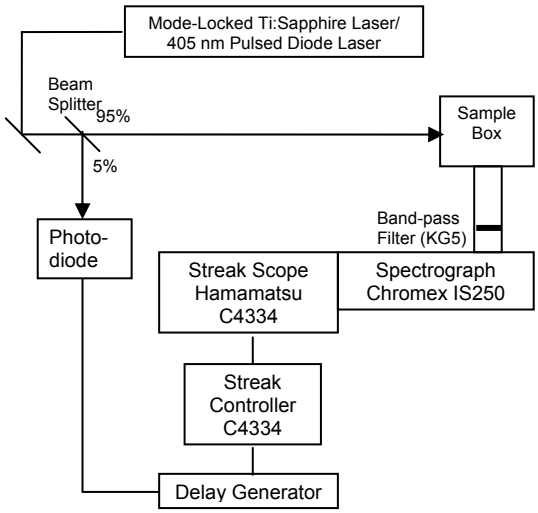

Figure 2-8 Streak camera experiment schematic; Excitation was provided by either a mode-locked Ti: Sapphire laser pulsing at 80MHz or a 405 nm diode laser pulsing at 1 MHz. The laser beam was used to focus at the center of the cuvette placed at the center of a light-tight sample box. The fluorescence emission was collected at 90 degrees to the excitation beam path and focused onto the entrance slit of a spectrograph. The streak camera was placed at the exit focal plane of the spectrograph. A computer workstation was used to control the spectrograph and the streak camera data acquisition.

The beam from the Ti: Sapphire laser was focused onto the cuvette using a 10X lens mounted on an xyz stage. A light-tight sample box was constructed to enclose the cuvette and lens, with an external beam dump to dispose of the unused portion of the beam. When using two-photon excitation at 800 nm, a band-pass filter (KG5, Schott) was placed in the beam path in the collection tube to block the scattered 800 nm light.

Excitation at 405 nm was accomplished with a diode laser pulsing at 1 MHz. There is minimal difference between 400 nm and 405 nm in the absorption of both drugs and no difference was observed in the results.

To calibrate the system and investigate its accuracy at retrieving lifetime information, a sample of rhodamine 6G was also measured using both 800 nm and 400 nm excitation. The rhodamine sample fluoresced much more brightly than the Photofrin® sample, making up for the poor collection efficiency of the system and yielding a much smoother curve (see Figure 2-9). Measurements were made over a spectral range of 570 nm to 586 nm, where the signal was most intense. Lifetimes were monoexponential, and found to be 3.4 ± 0.2 ns under 400 nm single-photon excitation and 3.7 ± 0.5 ns under 800 nm two-photon excitation, an insignificant difference. The lifetime of rhodamine 6G in methanol has been recorded as 4.13 ns, with an emission peak of 563 nm (Magde 2002).

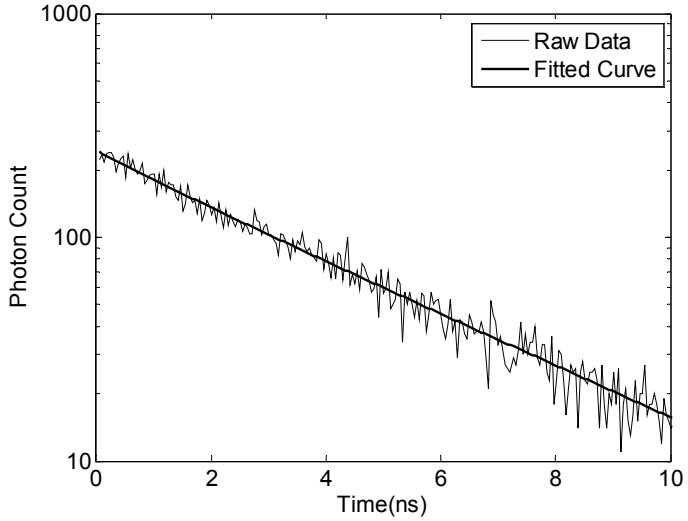

Figure 2-9 Typical fluorescence lifetime decay for rhodamine 6G, as measured with the streak camera. A lifetime of 3.4 ± 0.2 ns was found under 400 nm single-photon excitation and 3.7 ± 0.5 ns under 800 nm two-photon excitation.

2.6 Experimental Methods

The fluorescence lifetimes of Photofrin® (Axcan Pharma Inc., Mont-Saint-Hilaire, QC, Canada) and PpIX (Sigma-Aldrich Canada Ltd, Oakville, ON, Canada) dissolved in organic solvent solutions at known concentrations were investigated. For TCSPC spectroscopy experiments, Photofrin® was dissolved in methanol and PpIX was dissolved in dimethyl sulfoxide (DMSO) at concentrations ranging from 0.06 to 6 μg/ml and 0.1 to 10 μM, respectively. Solutions were mixed in 3 mL low fluorescence polystyrene cuvettes (CVD-VIS1S, Ocean Optics, Dunedin, FL, USA), which were then placed in the cuvette holder described in Section 2.3.

For measurements using the frequency domain Chronos lifetime spectrometer system, Photofrin® and PpIX and concentrations of around 0.06 μg/mL and 0.1 μM, respectively, were mixed in a quartz cuvette and compared against fluorescein as the standard. Note that concentrations of ALA and PpIX will be given in μM, which is the standard means of referring to concentration. Photofrin®, as it contains polymers of different lengths, has only a nominal molecular weight, thus conversion to μM would not be completely accurate. Photofrin® concentration will therefore be given in μg/mL.

For the streak camera measurements, Photofrin® at a concentration of 100 μg/mL in PBS was prepared in a quartz cuvette. PBS was not the optimal solvent for Photofrin®, which has a very poor quantum yield in PBS. However, this was

not discovered until well after the completion of the experiment, and the streak camera was no longer available.

2.7 Results

Eleven concentrations of Photofrin® (in methanol) and PpIX (in DMSO) ranging from 0.06 μg/ml to 6.0 μg/ml and 0.1 μM to 10 μM respectively were measured using the time-correlated single photon counting system described above. The data were analyzed using SigmaPlot (Systat Software Inc., San Jose, CA), which employed a Marquardt-Levenberg based algorithm that allowed fitting of decays with up to three exponentials and seven parameters. Deconvolution was not necessary as the time resolution of the system (200 ps) was sufficiently small compared to the measured lifetimes.

Photofrin® exhibited biexponential decay with an average lifetime of 10.0 ± 0.6 ns. These data were fitted with a biexponential decay calculated using four parameters, the amplitude and decay constant for each of the two exponentials. A slow component of 11.6 ± 0.5 ns was retrieved, as well as a fast lifetime component of 4.8 ± 0.9 ns, shown in Figure 2-10. Error bars represent one standard deviation from the fitted mean. The slow component likely corresponds to the monomer decay time, which Cubeddu *et al.* measured as 14.7 ns in buffer using single photon counting techniques, exciting with a mode-locked argon-ion laser tuned to 364 nm (Cubeddu 1986). The fast component is likely due to oligomers, aggregates, or photoproducts. Frequency domain

measurements obtained using the Chronos system also indicated biexponential decay, with long and short lifetimes of 10.5 ± 0.1 ns and 3.2 ± 0.2 ns being observed (Figure 2-11).

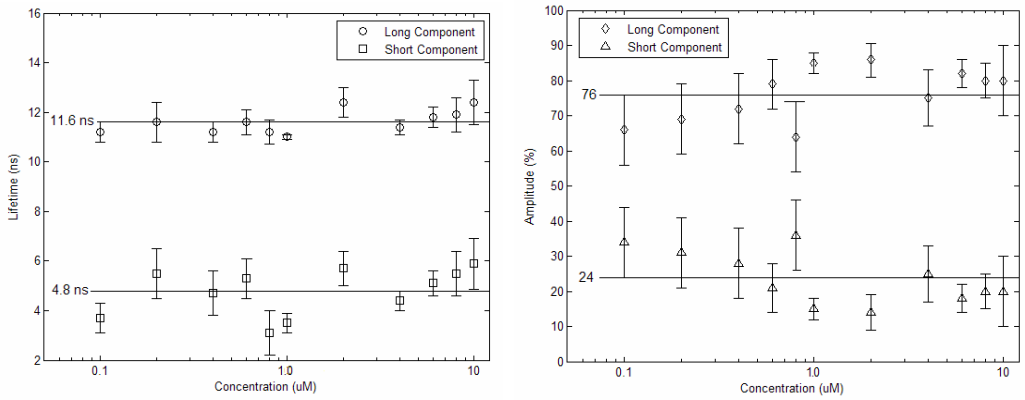

a) b)

Figure 2-10 a) Fluorescence lifetime and b) normalized coefficients of Photofrin® dissolved in methanol at different concentrations between 100 nM to 10 µM under 405 nm excitation. The decay was best fitted by a biexponential model. An average long component of 11.6 ± 0.5 ns with an average weighting of 76%, and an average short component of 4.8 ± 0.9 ns with an average weighting of 24% were found over this concentration range.

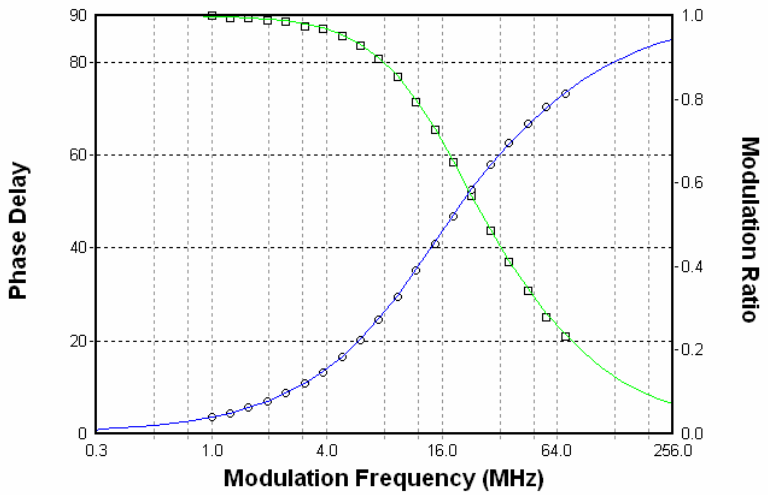

Figure 2-11 Frequency response for Photofrin® at 0.06 µg/ml taken using the frequency domain Chronos system. Squares denote the modulation and circles denote the phase delay. Long and short lifetimes of 10.5 ± 0.1 ns and 3.2 ± 0.2 ns were observed. Lifetimes were determined by fitting to the frequency response, performed automatically by the Vinci software, using non-linear least squares methods.

No concentration dependence was observed over this range. It should be noted that at high concentrations, quenching may occur, effectively reducing the lifetime. Conversely, other phenomena can occur at high concentrations, such as dimerization, reabsorption, and reemission, which serve to increase the observed lifetime. A sample of the spectral and lifetime data as gathered by the streak camera system is shown in Figure 2-12, and a summary of the measured lifetimes is shown in Figure 2-13.

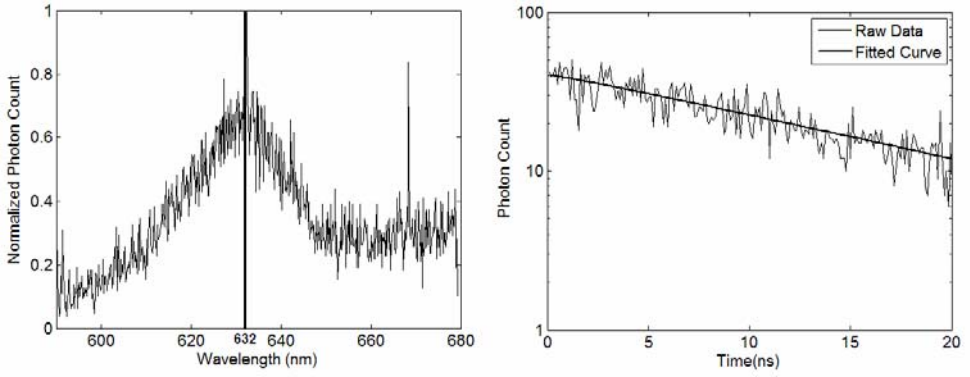

Figure 2-12 a) Emission spectrum for Photofrin® measured using the streak camera. The broad fluorescence emission peak is centered at 632 nm; b) Typical fluorescence lifetime decay for Photofrin® in PBS at 405 nm excitation, as measured with the streak camera. An average lifetime of 13.2 ± 2.0 ns was found.

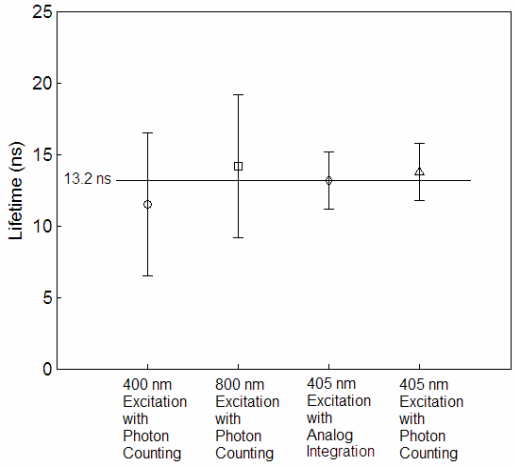

Figure 2-13 Summary of streak camera results for Photofrin® at a concentration of 100 µg/ml. An average lifetime of 13.2 ± 2.0 ns was found.

The curves exhibited monoexponential decay, fitted using the Trust-Region algorithm. The average lifetime was measured to be 13.2 ± 2.0 ns, independent of the nature of the excitation, indicating that the two-photon excitation scheme used for the FLIM experiments in cells would not affect the measured lifetime.

PpIX was found to exhibit monoexponential decay with an average lifetime of 16.4 ± 0.2 ns, seen in Figure 2-14. This compared well with a frequency domain measurement taken using the Chronos system, which measured a fluorescence lifetime of 16.2 ± 0.1 ns (see Figure 2-15). It is also in agreement with the findings of Brancaleon *et al.*, who observed a lifetime of 16.8 ± 0.6 ns in DMSO, using time correlated single photon counting, exciting with a pulsed diode laser head at 393 nm (Brancaleon 2003). Again, no significant concentration dependence was observed over the range investigated.

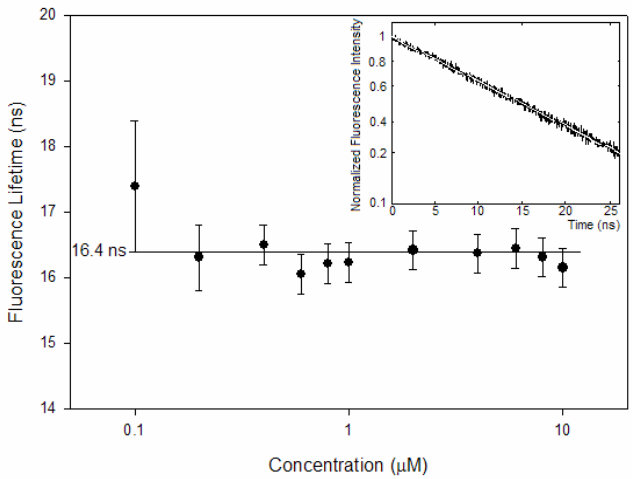

Figure 2-14 Fluorescence lifetime of PpIX (in DMSO) at different concentrations between 100 nM to 10 μM under 405 nm excitation. An average lifetime of 16.4 ± 0.2 ns was found over this concentration range; the inset shows a typical fluorescence lifetime decay fit by a Marquardt-Levenberg algorithm for a concentration of 2 μM. Decay was best fit by a mono-exponential.

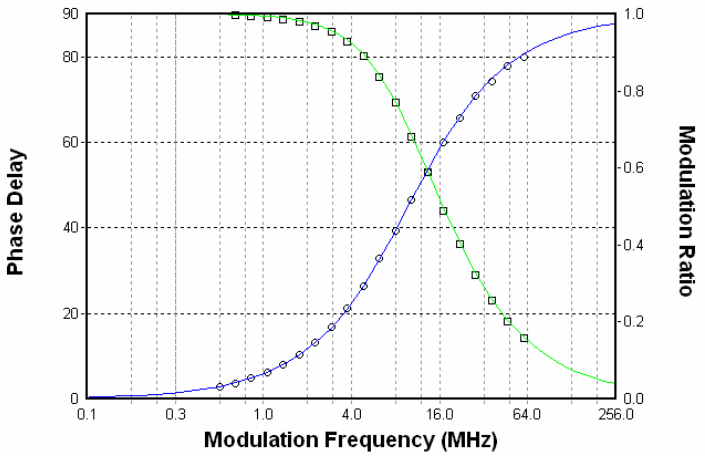

Figure 2-15 Frequency response for PpIX at 0.1 μM taken using the frequency domain Chronos system. Squares denote the modulation and circles denote the phase delay. A lifetime of 16.2 ± 0.1 ns was observed. Lifetimes were determined by fitting to the frequency response, performed automatically by the Vinci software, using non-linear least squares methods.

In addition to the experiments with the 405 nm diode laser, measurements were taken of Photofrin® and PpIX using 635 nm excitation with a pulsed laser (BHL-150, Becker & Hickl GmbH) which had a pulse width of approximately 150 ps at FWHM and a repetition rate of 50 MHz. A time resolution of nearly 500 ps was determined by measuring the full width at half maximum (FWHM) of the IRF. The set-up was identical to that of the 405 nm experiments, however a 645 nm longpass filter was used instead of the 580 nm one. Photofrin® was measured in methanol at concentrations of 14.3 μg/ml and 71.4 μg/ml, each in triplicate, and a biexponential decay was observed. An average long component of 12.3 ± 0.6 ns, and an average short component of 4.1 ± 0.5 ns were found, with no difference observed between the two concentrations. Figure 2-16 shows the decay for Photofrin® at 71.4 μg/ml. PpIX was measured in methanol at concentrations ranging between 8.0 μM and 78 μM and was found to exhibit a

decay that was biexponential, largely dominated by the long component which averaged at 11.1 ± 0.6 ns with a smaller contribution from the short component of 0.38 ± 0.05 ns. The results are shown in Figure 2-17.

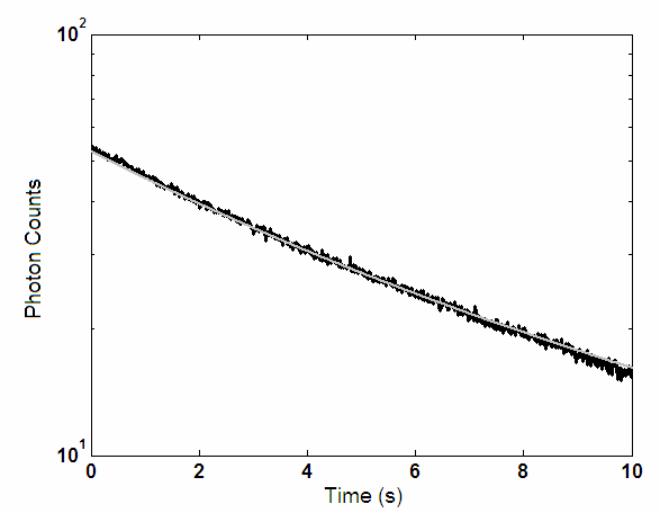

Figure 2-16 Fluorescence decay for Photofrin® at a concentration of 71.4 ug/ml in methanol under 635 nm excitation. A long component of 12.3 ± 0.6 ns and a short component of 4.1 ± 0.5 ns were found as the average of the results for Photofrin® at these two concentrations.

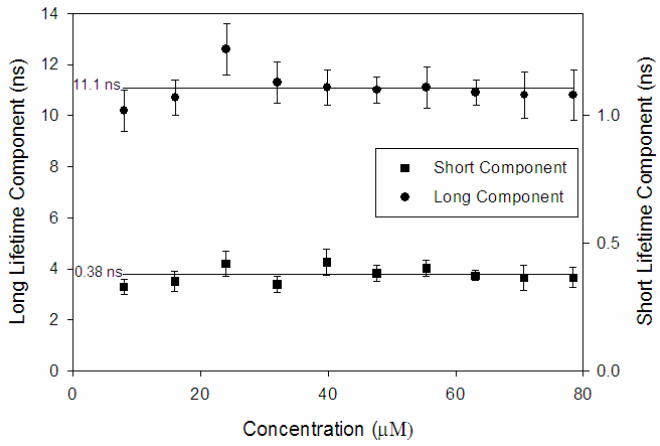

Figure 2-17 Fluorescence decay for PpIX at a concentrations between 8.0 and 78 μM under 635 nm excitation. An average long component of 11.1 ± 0.6 ns and an average short component of 0.38 ± 0.05 ns were found.

Chapter III – Fluorescence Lifetime Measurements In Cells

3.1 Cell Culture and Slide Preparation

Drug localization and fluorescence lifetime of Photofrin® and ALA-induced PpIX were investigated in Mat-LyLu (MLL) rat prostate adenocarcinoma cells *in vitro*, a cell line used in previous studies (Dysart 2005, Dysart 2006). These cells were grown in 50 mL vials with 3.5 mL of media and incubated at 38ºC in a water jacketed CO_2 incubator (Forma Series II, Thermo Fisher Scientific Inc, Waltham, MA, USA). Media consisted of RPMI medium 1640 (Gibco-BRL, Gaithersburg, MD, USA) supplemented with 10% Fetal Bovine Serum (FBS) (Gibco-BRL, Gaithersburg, MD, USA), 2% antibiotic/antimycotic (Gibco-BRL, Gaithersburg, MD, USA) to help protect against contamination, and 1% hepes buffer to maintain the pH (Dysart 2006). This cell line exhibits a 15 hour doubling time, and cells were passaged every 24 to 48 hours. To passage, the medium was pipetted out of the vial and cells were rinsed once with 3 mL of PBS. The PBS was pipetted out, and cells were trypsinized with 0.8 mL of 0.5% 10X Trypsin-EDTA (Gibco-BRL, Gaithersburg, MD, USA) for 1 minute to allow cells to detach. 2 mL of medium were then added to the vial to neutralize the trypsin. The resulting mixture, now containing detached cells, was pipetted out and small amounts (on the order of 0.2 to 0.5 mL) were distributed into one or two new vials. 3.5 mL of medium were then added to these vials, which were labeled and placed in the incubator.

For imaging, cells were plated on 25 mm glass coverslips in 35x10 mm petri dishes and incubated for a minimum of 6 hours in 2 mL of medium to allow attachment before the medium was replaced with 2 mL of prepared medium containing the photosensitizer.

For incubation with Photofrin®, a stock solution of 2.5 mg/mL of the photosensitizer dissolved in PBS was prepared and diluted into RPMI medium supplemented with 10% FBS, 2% antibiotic/antimycotic and 1% hepes buffer, to a concentration of 10 μg/mL (Dysart 2005). Cells were incubated in this medium for 18 hours prior to imaging (Dysart 2005).

For incubation with ALA, the medium was prepared by diluting a stock solution of 96 mM of ALA in DMSO into RPMI medium supplemented with 2% antibiotic/antimycotic and 1% hepes buffer, to a concentration of 10 mM (Dysart 2006). Growth medium was removed from the dishes and cells were rinsed with PBS before the prepared medium was added. Note that the prepared medium did not include FBS, as it interferes with the uptake of ALA. Cells were incubated in this medium for 3.5 hours before imaging (Dysart 2006).

After incubating for the appropriate time with each photosensitizer, the coverslips were rinsed with PBS, placed in a bracket for imaging and bathed in 1 mL PBS to prevent the cells from drying out during imaging.

3.2 FLIM System

Fluorescence lifetime imaging was performed using an inverted multiphoton fluorescence microscope (TSC SP5 & DMI 6000 B, Leica, Wetzlar, Germany), which had an integrated TCSPC based FLIM module (SPC-830, Becker & Hickl GmbH, Berlin, Germany). FLIM data were analyzed using the built-in software (SPCImage v2.8.3.2921, Becker & Hickl). The schematic of the system is shown in Figure 3-1. A Ti: Sapphire laser (Chameleon-Ultra, Coherent, Santa Clara, CA, USA) provided two photon excitation at 810 nm, pulsing at 80 MHz. The emission spectra selection in this system was done through a prism-based spectrometer that allowed continuous tuning from the near UV to the near IR.

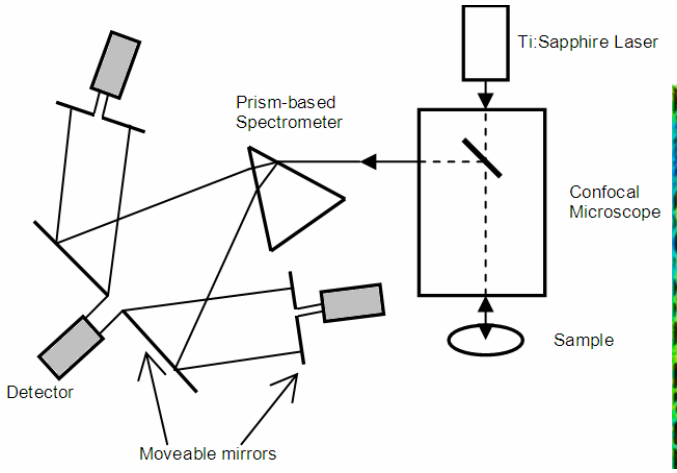

a)

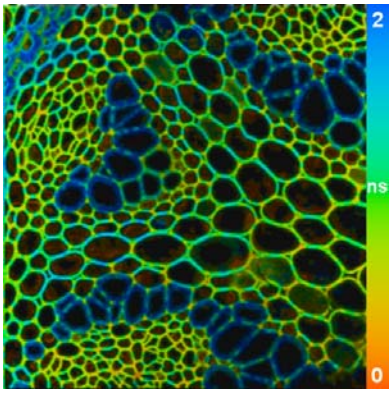

b)

Figure 3-1 a) Schematic for the fluorescence lifetime imaging system. The cell sample was excited by a Ti:Sapphire laser emitting at 810 nm. Imaging was performed using a confocal microscope. The emission filter in this system is a prism-based spectrometer that allows for continuous tuning from the near UV to the near IR, with four separate channels and four separate detectors (only three shown here), for simultaneously confocal imaging at four spectral channels. For fluorescence lifetime imaging, only two channels may be active. The light emitted by the sample is dispersed by the prism. The spectrum is sectioned as desired by software-controlled adjustment of the moveable mirrors, and those sections of the spectrum are received by separate detectors. Adapted from Borlinghaus 2006; b) Fluorescence lifetime image of the Rhizome of *Convallaria majalis* taken using this system for spectral and temporal calibration.

The excitation mode in this system relied on two-photon absorption. All clinical PDT to date uses one-photon excitation (Wilson 2006), the energy of which must fall into an absorptive region for the photosensitizer. A two-photon absorption process involves the simultaneous absorption of two photons of longer wavelengths, the probability of which depends on the square of the local light intensity. This results in more localized activation than one-photon excitation, which improves targeting and may have applications in treatments where a high degree of specificity is required, such as in the treatment of age-related macular degeneration (Wilson 2006).

Excitation via the two-photon process requires that each of the simultaneously absorbed photons possess half the energy, and therefore double the wavelength, of the single photon that would be required for the same excitation (Wilson 2006). Figure 3-2 shows an energy level diagram describing this process.

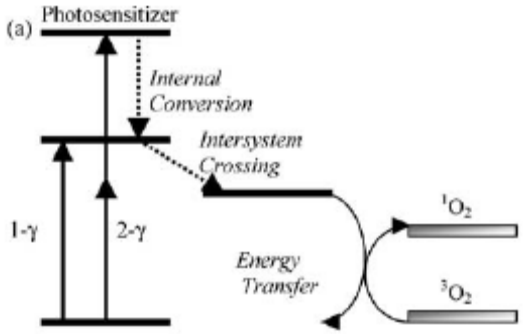

Figure 3-2 Simplified Jablonski diagram describing two-photon excitation of a photosensitizer, followed by subsequent energy transfer to excite oxygen to its singlet state (Wilson 2006)

3.3 Validation

To validate the use of the FLIM microscope and two-photon excitation, an experiment was conducted using Photofrin® dissolved in methanol to compare the measured fluorescence lifetime with lifetimes previously obtained by TCSPC spectroscopy and one-photon excitation. Photofrin® at a concentration of 100 ug/mL was prepared in methanol. For imaging, a blank glass coverslip was placed in a bracket for imaging and 1.5 mL of the Photofrin® solution was placed inside of it. By marking the underside of the coverslip for a point of reference, the microscope was focused at a point in the solution just inside the glass. Excitation was provided by the Ti:Sapphire laser, observations were made in the spectral window of 600 to 750 nm, and a collection time of 60 s was used. A biexponential decay was found, where the fast component of 3.5 ± 0.5 ns with a weighting of 36% and the slow component of 11.9 ± 1.1 ns with a weighting of 64% agree with those found using TCSPC (4.8 ± 0.9 ns and 11.6 ± 0.5 ns) and the Chronos system (3.2 ± 0.2 ns and 10.5 ± 0.1 ns). Figure 3-3 shows the lifetime distribution histograms for these two components.

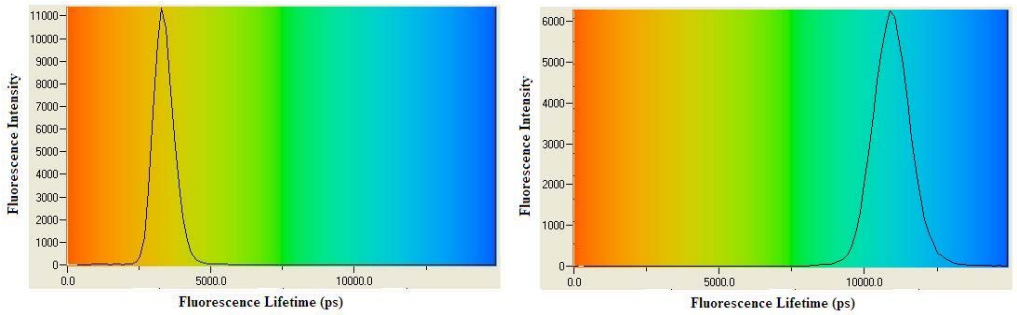

a) b)

Figure 3-3 Fluorescence lifetime distribution histograms for a) the fast component (3.5 ± 0.5 ns) and b) the slow component (11.9 ± 1.1 ns) of the biexponential decay measured with the FLIM system for Photofrin® in methanol.

3.4 Initial Lifetime Measurements

Emitted fluorescence was monitored over 600 – 750 nm for collection times of 100 s, 150 s and 300 s for Photofrin®-incubated cells, PpIX-incubated cells, and unstained cells, respectively. Confocal and differential interference contrast (DIC) images were also acquired for each imaged cell group. The software controls for the filter wheel, offset and modulator of the multiphoton (MP) laser were set to 40%, 26% and 81%, respectively. Images were 512x512 pixels and the scan speed was 400 Hz. Note that, since there is no communication between the workstations that control the confocal microscope and the FLIM acquisition system, it is up to the user to manually ensure that the frame size and scan speed are set to the same values on both systems.

The steady-state fluorescence images were acquired in two spectral bands: a green channel from 480-570 nm where autofluorescence is strongest, and a red channel from 600-750 nm, the spectral emission region of the photosensitizers under investigation. In unstained cells, autofluorescence observed in the green channel was attributed to flavins such as riboflavin, flavin mononucleotide (FMN) and flavin adenine dinucleotide (FAD), which fluoresce around 525 nm. FMN exhibits a fluorescence lifetime of 4.7 ns, while FAD has a lifetime of 2.3 ns (Lakowicz 1999). Signal collected by the red channel appears to be autofluorescence of the mitochondria. A fluorescence peak at 2.6 ± 0.7 ns (errors determined from FWHM of the peak in the histogram) was measured from autofluorescence over the 600-750 nm region. The fluorescence lifetime

distribution histogram for the unstained cells indicated that most cellular autofluorescence occurred below 4 ns, as shown in Figure 3-4. A large peak was observed at 1.0 ± 0.1 ns, which is believed to be autofluorescence attributed mostly to NADH, which has an emission peak around 460 nm and is known to exhibit a lifetime near 0.3 ns in aqueous buffer, and 1.2 ns when bound to protein (Lakowicz 1999).

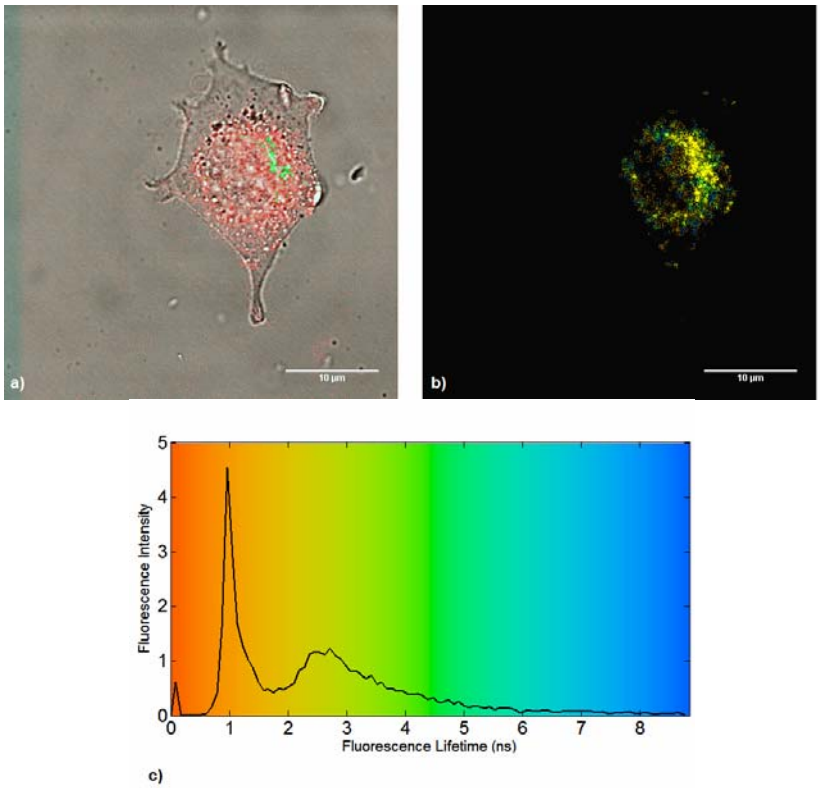

Figure 3-4 Unstained cells; (a) Merged steady-state fluorescence-DIC image. Green signal indicates autofluorescence of flavins, and the red signal indicates autofluorescence of the mitochondria; (b) Fluorescence lifetime image; (c) Fluorescence lifetime distribution histogram over the whole image. Autofluorescence exhibited an average lifetime peak of 2.6 ± 0.7 ns.

Cells incubated with ALA to induce PpIX were similarly imaged, and were found to exhibit an average lifetime of 6.3 ± 1.2 ns. This corresponds to light blue in the false colour scheme, as seen on the lifetime histogram (Figure 3-5).

The light blue pixels in the fluorescence lifetime image appear to be co-localized with the red signal in the steady-state-DIC image, seen in Figure 3-5, which originates from PpIX fluorescence.

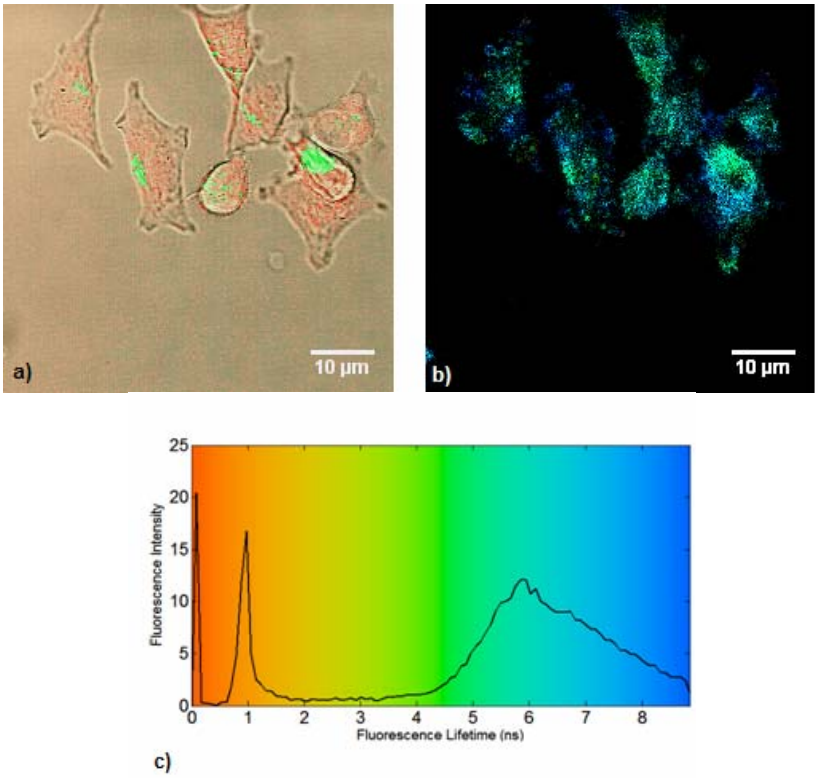

Figure 3-5 MLL cells incubated with ALA at 10µM for 4 hours; (a) Merged steady-state fluorescence-DIC image. Green signal indicates flavinoid autofluorescence, and the red signal indicates location of the photosensitizer; (b) Fluorescence lifetime image; (c) Fluorescence lifetime distribution histogram. PpIX exhibited an average lifetime peak of 6.3 ± 1.2 ns.

Cells incubated with Photofrin® were also imaged, and exhibited an average lifetime of 5.5 ± 1.2 ns, as shown in Figure 3-6. The pixels corresponding to the photosensitizer in the fluorescence lifetime image are again co-localized with the red signal of the steady-state fluorescence-DIC image, which originates from Photofrin® fluorescence.

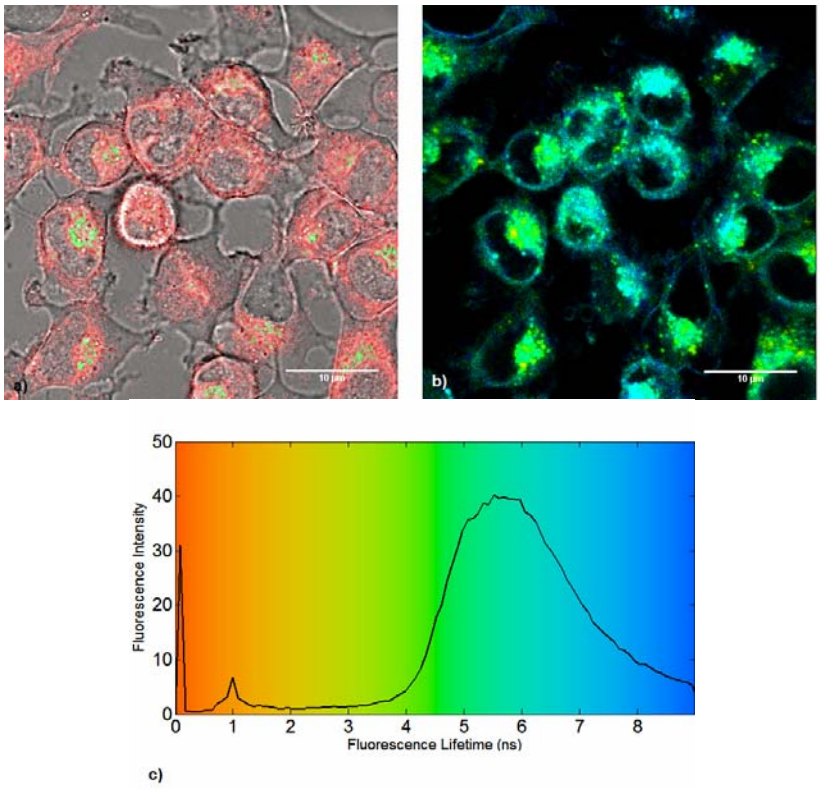

Figure 3-6 MLL cells incubated with Photofrin®: (a) Merged steady-state fluorescence-DIC image. Green signal indicates flavinoid autofluorescence, and the red signal indicates location of the photosensitizer; (b) Fluorescence lifetime image; (c) Fluorescence lifetime distribution histogram. Photofrin® exhibited an average lifetime peak of 5.5 ± 1.2 ns.

The average fluorescence lifetimes exhibited by Photofrin® and ALA-induced PpIX in MLL cells were both significantly longer than the lifetimes resulting from cellular autofluorescence, illustrated in Figure 3-7, where the three lifetime histograms appear together, scaled for the NADH autofluorescence that occurs near 1 ns. There is virtually no autofluorescence observed with a lifetime above ~4 ns, while the lifetime peaks of the two photosensitizers occur well above 5 ns. It should also be noted that the intensity of the autofluorescence is low compared to the photosensitizers, even at its peak of 2.6 ns. This suggests that the use of time-gated fluorescence for monitoring photodynamic therapy drugs *in vivo*

has potential, as interference from tissue autofluorescence will be so minimal as to be negligible. Additionally, separating the autofluorescence signal and that from the photosensitizer *in vivo* (even though the intrinsic fluorescence is a fraction of the photosensitizer) may improve attempts to quantify the photosensitizer concentration, as a component of a comprehensive model of photodynamic dose.

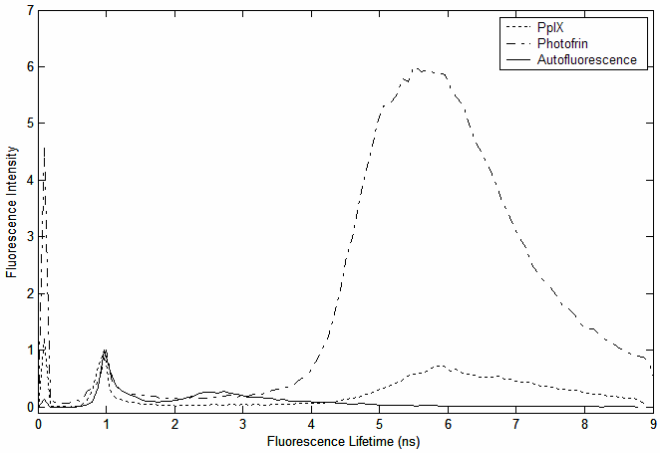

Figure 3-7 Fluorescence lifetime distribution histograms for unstained cells (solid), cells incubated with ALA to induce PpIX (dotted) and cells incubated with Photofrin® (dot-dashed). Lifetimes of photosensitizers are significantly longer than autofluorescence lifetimes, and autofluorescence above 4 ns is negligible compared to the intensities of the fluorescence of the photosensitizers.

3.5 Photobleaching and Photoproduct Generation Studies

Preliminary lifetime measurements were directed at 600-750 nm, the entire spectral region from which fluorescence from these drugs is expected. Fluorescence was next measured in two separate spectral windows: channel 1 observed 620 – 645 nm to capture the main fluorescence peak centered near 635 nm, and channel 2 observed either 650 – 670 nm for Photofrin® or 670 – 690 nm for PpIX, to capture the fluorescence of photoproducts and aggregates.

The software controls for the filter wheel, offset and modulator of the MP laser were set to 25%, 40% and 80%, respectively. Images were 128x128 pixels, to reduce the acquisition time required, and the scan speed was 400 Hz. The acquisition times used were 10 s for Photofrin®, and 15 s for PpIX. Photofrin® was incubated at 10 μg/ml and ALA at 10.9 mM.

Data for each cell group were gathered in series, with each series containing three FLIM acquisitions taken consecutively. The series were collected in two ways. The first involved the three acquisitions being taken one directly after the other, with no interruption in excitation light. The second incorporated a dark period between each of the consecutive acquisitions, with the duration of the dark period matching the acquisition time, to investigate the effects of fractionation of light delivery on measured lifetime. This was accomplished by setting the SPC-830 software to acquire 5 data sets consecutively, and manually shuttering the excitation light via the controls on the confocal microscope workstation during the second and fourth acquisitions. Average lifetimes were found as follows.

Table 3.1 Average lifetimes for Photofrin® under 10 s consecutive acquisitions and acquisitions interrupted by dark periods

Photofrin®	First Acquisition		Second Acquisition		Third Acquisition	
	chan 1	chan 2	chan 1	chan 2	chan 1	chan 2
Consecutive Acquisition	7.8 ± 0.5	5.1 ± 0.4	6.8 ± 0.7	4.7 ± 0.5	6.6 ± 0.6	4.9 ± 0.5
Dark Period Acquisition			6.8 ± 0.6	4.6 ± 0.5	6.2 ± 0.5	4.6 ± 0.5

Figures 3-8 and 3-9 show the results for Photofrin®, for consecutive acquisition and acquisition with alternating dark periods, respectively. There was no significant difference between the observed lifetimes for consecutive acquisition and acquisition with dark periods. No significant difference was observed in the lifetime measured by channel 2 – the photoproduct lifetime – between subsequent acquisitions. The only significant difference lies in channel 1 – the main Photofrin® peak – between the first and second acquisitions. This trend is also seen in the results for PpIX, presented below. Results for PpIX are found in Figures 3-10 and 3-11, for consecutive acquisition, and acquisition with alternating dark periods, respectively.

Table 3.2 Average lifetimes for PpIX under 105s consecutive acquisitions and acquisitions interrupted by dark periods

PpIX	First Acquisition		Second Acquisition		Third Acquisition	
	chan 1	chan 2	chan 1	chan 2	chan 1	chan 2
Consecutive Acquisition	10.8 ± 1.7	6.3 ± 1.0	8.2 ± 1.1	6.1 ± 0.9	8.4 ± 1.2	6.0 ± 1.2
Dark Period Acquisition			8.8 ± 1.6	5.5 ± 0.8	8.1 ± 1.4	5.7 ± 1.0

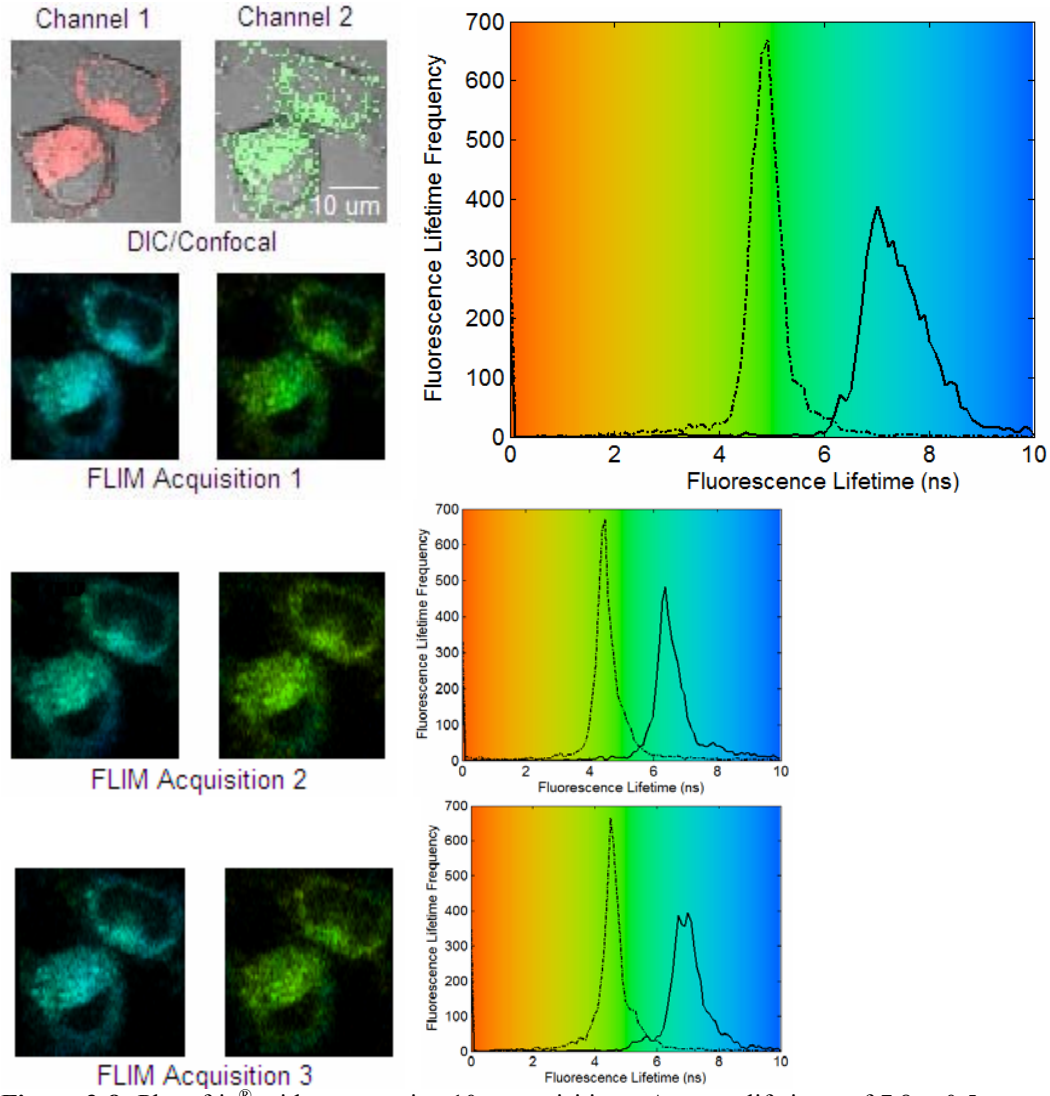

Figure 3-8 Photofrin® with consecutive 10 s acquisitions. Average lifetimes of 7.8 ± 0.5 ns and 5.1 ± 0.4 ns were measured with channel 1 and channel 2 respectively for the first acquisition, 6.8 ± 0.7 ns and 4.7 ± 0.5 ns for the second acquisition, and 6.6 ± 0.6 ns and 4.9 ± 0.5 ns for the third acquisition.

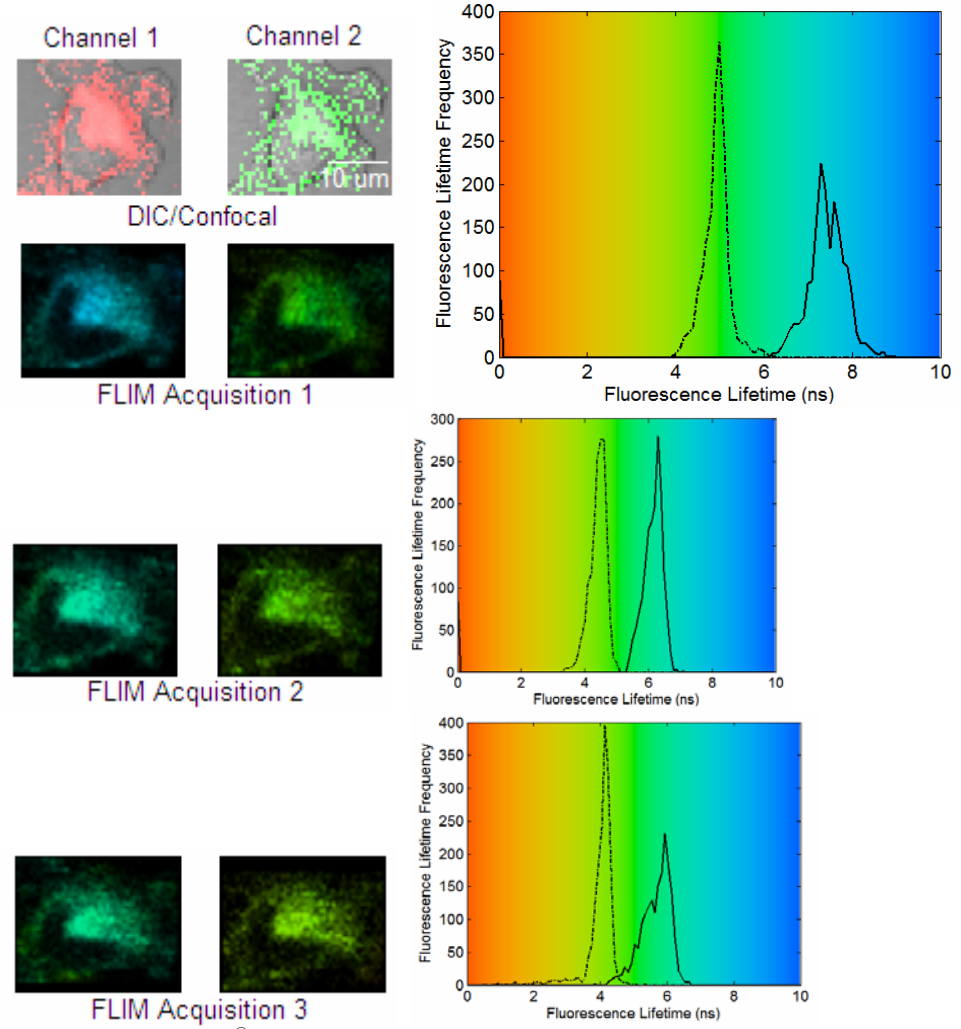

Figure 3-9 Photofrin® with 10 s dark periods between each 10 s acquisition. Average lifetimes of 7.8 ± 0.5 ns and 5.1 ± 0.4 ns were measured with channel 1 and channel 2 respectively for the first acquisition, 6.8 ± 0.6 ns and 4.6 ± 0.5 ns for the second acquisition, and 6.2 ± 0.5 ns and 4.6 ± 0.5 ns for the third acquisition.

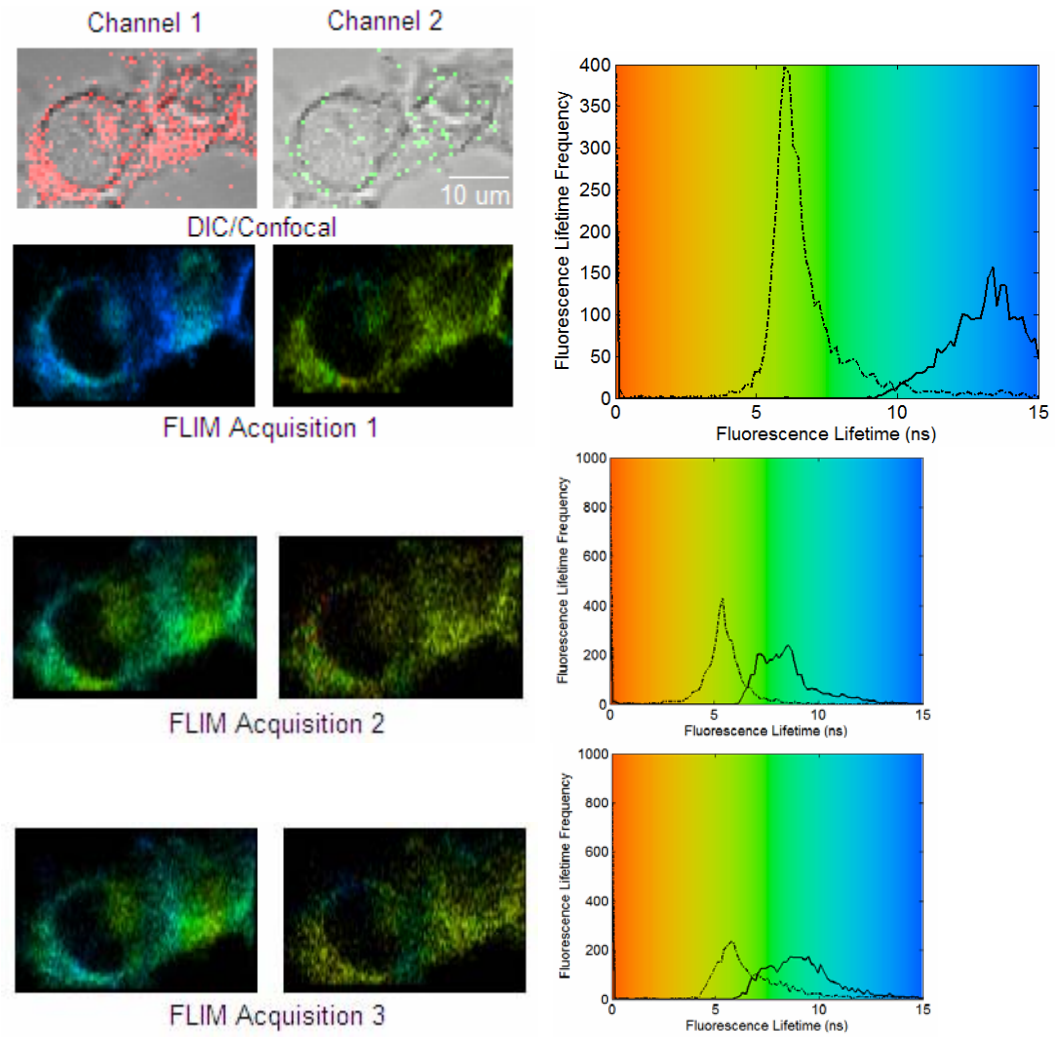

Figure 3-10 PpIX with consecutive 15 s acquisitions. Average lifetimes of 10.8 ± 1.7 ns and 6.3 ± 1.0 ns were measured with channel 1 and channel 2 respectively for the first acquisition, 8.2 ± 1.1 ns and 6.1 ± 0.9 ns for the second acquisition, and 8.4 ± 1.2 ns and 6.0 ± 1.2 ns for the third acquisition.

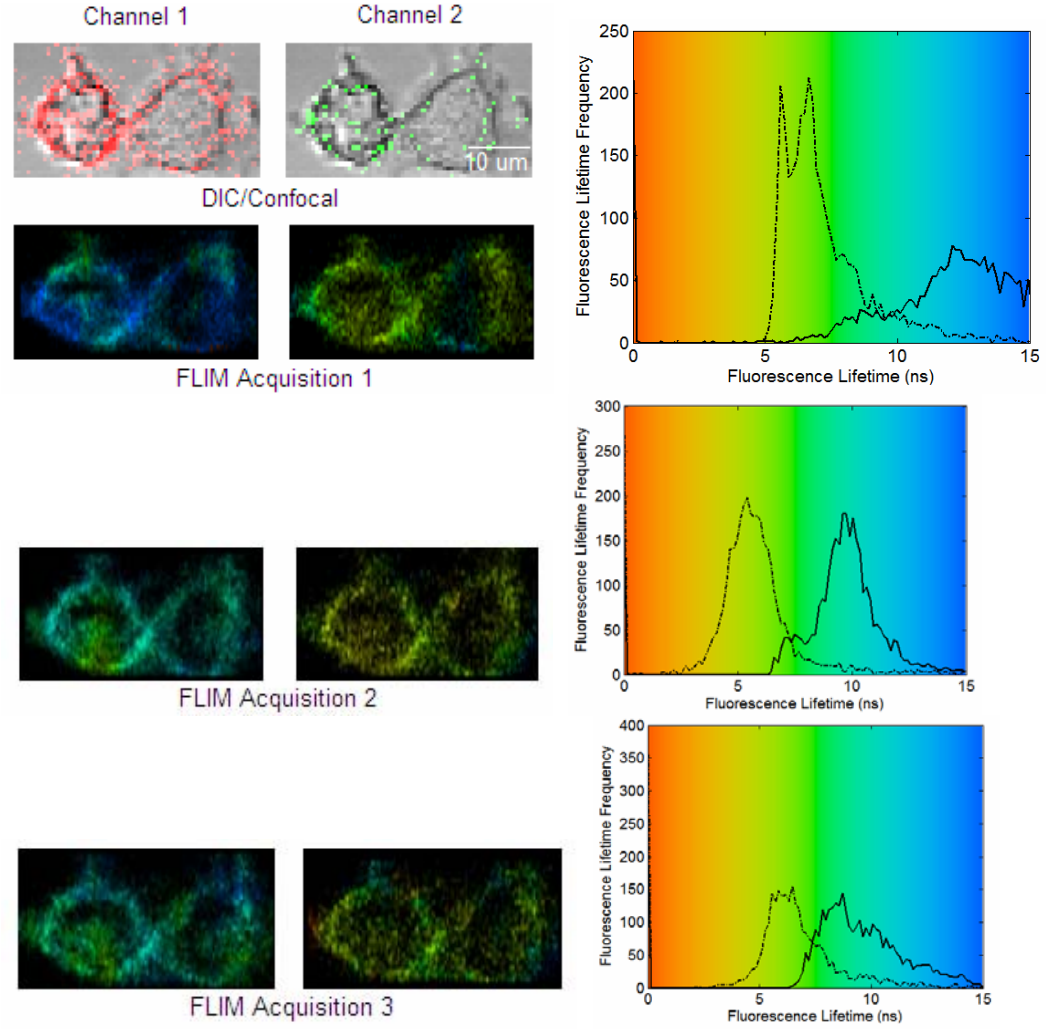

Figure 3-11 PpIX with 15 s dark periods between each 15 s acquisition. Average lifetimes of 10.8 ± 1.7 ns and 6.3 ± 1.0 ns were measured with channel 1 and channel 2 respectively for the first acquisition, 8.8 ± 1.6 ns and 5.5 ± 0.8 ns for the second acquisition, and 8.1 ± 1.4 ns and 5.7 ± 1.0 ns for the third acquisition.

3.6 Co-localization Studies

While this study has observed, and it has been noted in the literature that Photofrin® and ALA-induced PpIX accumulate in the mitochondria (Kress 2003), large doses of photosensitizer may result in variable accumulation in cells. For example, a sufficiently large dose of ALA may result in PpIX leaking out of the mitochondria and into the cytoplasm. To ensure that both Photofrin® and PpIX were accumulating in the mitochondria for the incubation concentrations used, co-localization studies were performed. Cells were first incubated with concentrations of either Photofrin® or PpIX as described above. After the incubation period, cells were washed twice with PBS and incubated with 100 nM of MitoTracker Green (a mitochondria-specific fluorescent stain) in FBS-free media for 40 minutes. Cells were then washed three times with PBS and imaged. Confocal images were acquired with the Leica system used above, first under 488 nm excitation, which corresponds with an absorptive region of MitoTracker Green, and then under 514 nm light, which corresponds to an absorption peak for both Photofrin® and PpIX. Channel 1 observed the emissions from MitoTracker Green under 488 nm excitation, covering a spectral region of 500 – 540 nm; channel 2 observed emissions from the drugs under 514 nm excitation, over the spectral region of 600 – 750 nm. Images were 512x512 pixels and acquired at 400 Hz.

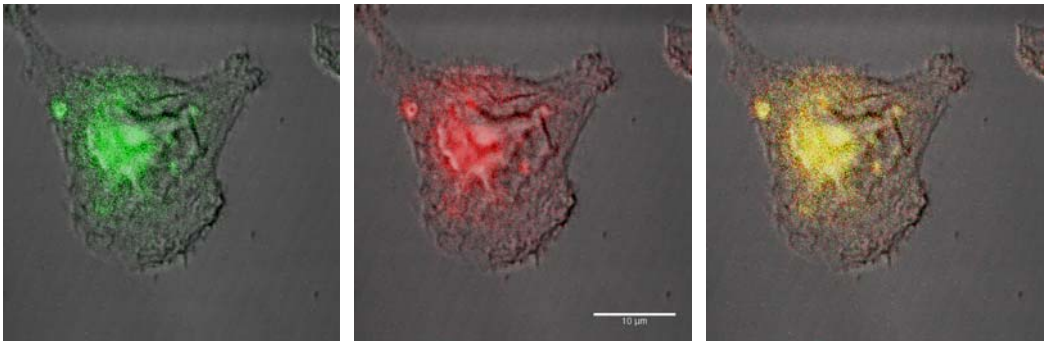

a) b) c)

Figure 3-12 a) MitoTracker Green fluorescence over 500 – 540 nm. The peak emission is at 515 nm; b) Fluorescence from Photofrin® over 600 – 750 nm; c) Result of a merge between a) and b). Yellow pixels are observed wherever a green pixel and a red pixel overlap.

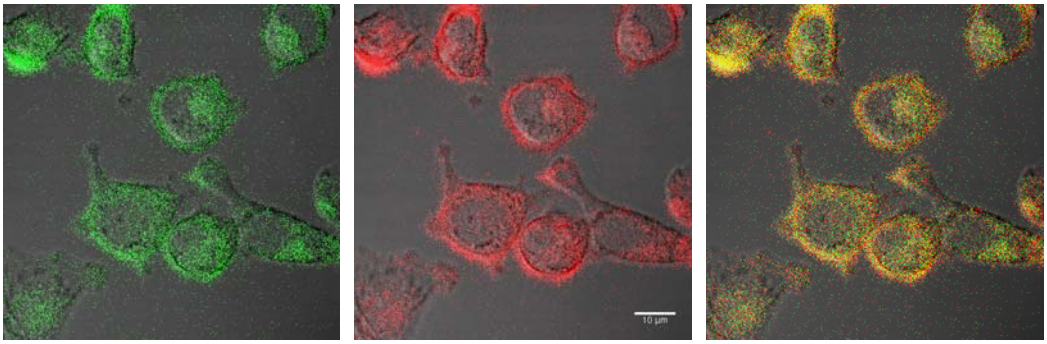

a) b) c)

Figure 3-13 a) MitoTracker Green fluorescence over 500 – 540 nm. The peak emission is at 515 nm; b) Fluorescence from PpIX over 600 – 750 nm; c) Result of a merge between a) and b). Yellow pixels are observed wherever a green pixel and a red pixel overlap.

As can be seen in Figures 3-12 and 3-13, the signals arising from both Photofrin® and PpIX co-localize very well with those from the MitoTracker Green, indicating that both drugs do indeed localize in the mitochondria at the concentrations used.

Chapter IV – Discussion and Conclusions

4.1 General Discussion of Results

Fluorescence lifetime is a sensitive indicator of a fluorophore's binding and its local environment. Many fluorophores display significantly different fluorescence characteristics when they bind to other molecules. Therefore, using FLIM to study localized photosensitizer lifetime is a useful approach as it provides location-specific information compared to traditional measurements of bulk solutions or cellular suspensions.

In this study, two sets of *in vitro* measurements of fluorescence lifetimes of Photofrin® and ALA-induced PpIX have been performed in living MLL cells using a two-photon FLIM system; one observing the broad spectral region from 600 – 750 nm, and the second observing two narrower spectral windows. For Photofrin®, these windows were between 620 – 645 nm and 650 – 670 nm; for PpIX, 620 – 645 nm and 670 – 690 nm (see Figures 4-1 and 4-2). These windows were selected to capture the main fluorescence peak, centered around 630 nm, as well as the fluorescence of the major photoproducts and aggregates. For the first experiment involving the broad spectral window, lifetimes of both photosensitizers localized in cells were found to be significantly shorter compared to the lifetime measured in bulk photosensitizer solutions. The shorter lifetime (6.3 ns, see Figure 3-5 and Table 4.1) of localized ALA-induced PpIX in cells agrees fairly well with literature values (Kress 2003). The average lifetime of

Photofrin® in cells (5.5 ns, see Figure 3-6 and Table 4.1), however, is significantly shorter than what has been reported by others (~13 ns) (Ruck 2001, Konig 1990).

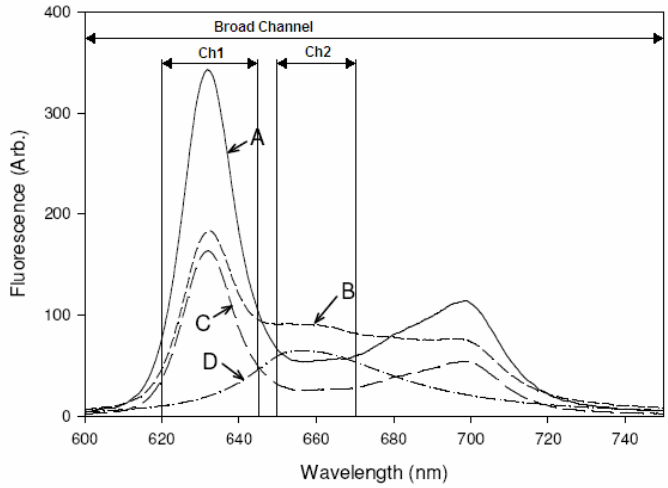

Figure 4-1 Fluorescence emission spectrum of Photofrin® showing detection windows. Emission spectra of Photofrin® before PDT (A), the resulting spectrum after PDT (B) consisting of Photofrin® (C) with photoproduct (D) centered at 658nm (adapted from Dysart 2005)

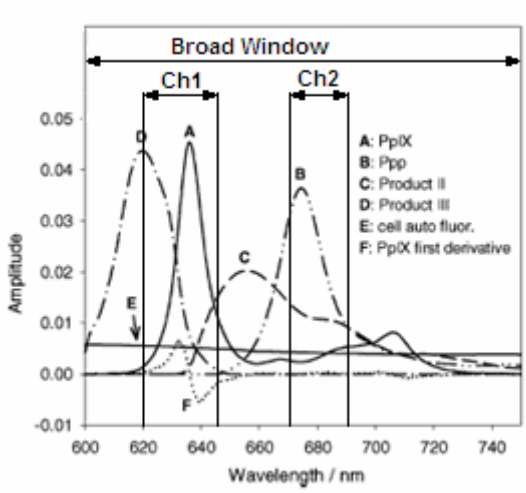

Figure 4-2 Fluorescence emission spectrum of PpIX showing detection windows (adapted from Dysart 2006)

In order to verify the instrumentation and methods used for lifetime measurements, experiments were performed on Photofrin® solutions using a

streak camera and compared to the FLIM system, as discussed in Chapter 2. Both results were consistent with the TCSPC measurements. The results for the FLIM measurements of ALA-induced PpIX in MLL cells confirmed that the method used for the intracellular measurements was sound (Kress 2003).

In the second experiment, with the two narrower spectral windows, shorter lifetimes were again observed as compared to the solution measurements. Interestingly, the estimated lifetime values for the photoproducts and/or aggregates in this experiment were not significantly different from the lifetime values measured over 600 – 750 nm (see Table 4.1), suggesting that it was in fact predominantly photoproduct and aggregate fluorescence that was being captured over that broad spectral range. Acquisition times were 10 times longer for the 600 – 750 nm measurement as opposed to the two channel experiment, thus it is plausible that significant photoproduct generation occurred, and the overall intensity of the main peak decreased. Lifetimes measured over the main fluorescence peak for both photosensitizers in the two channel experiment were found to be significantly longer than the photoproduct/aggregate lifetimes in both cases (see Tables 3-1, 3-2). While the lifetime values for PpIX, both over the main fluorescence peak and the photoproduct peak, appear to make sense when compared with literature values (see Table 4.1) given the varying nature of the tissue or cells under investigation, the results for Photofrin® are still much lower than expected, with the main fluorescence peak yielding a lifetime of only 7.8 ± 0.5 ns while the expected lifetime is around 13 ns.

Table 4.1 Summary of Experimental and Literature Fluorescence Lifetime Values for Photofrin® and ALA-induced PpIX

Lifetime (ns)	PpIX	Photofrin
in Organic Solution Time Domain (Bulk measurement)	16.4 ± 0.2	10.0 ± 0.6 τ_1: 4.8 ± 0.9 τ_2: 11.6 ± 0.5
in Organic Solution Time Domain (FLIM)	--	9.9 ± 1.2 τ_1: 3.5 ± 0.5 τ_2: 11.9 ± 1.1
in Organic Solution Frequency Domain (Chronos)	16.2 ± 0.1	8.9 ± 0.1 τ_1: 3.2 ± 0.2 τ_2: 10.5 ± 0.1
in Organic Solution Literature Values	16.8 ± 0.6 (Brancaleon 2003)	14.7 (Cubeddu 1986)
in MLL Cells One Channel (FLIM)	6.3 ± 1.2	5.5 ± 1.2
in MLL Cells Two Channels (FLIM)	monomeric: 10.8 ± 1.7 aggregates: 6.3 ± 1.0	monomeric: 7.8 ± 0.5 aggregates: 5.1 ± 0.4
in Cells Literature Values	monomeric: 7.44 ± 0.56 (Kress 2003) 17 (Konig 1993) 18~20 (Kress 2003) 12.1~14.5 (Kress 2003) aggregates: 3.6 ± 0.46 (Kress 2003) 5 (Konig 1993) 6 (Kress 2003) 5.4 (Theodossiou 2002)	monomeric: 13.3 ± 0.3 (Ruck 2007) 13.2 ± 2 (Konig 1990) aggregates: 8.0 ± 0.6 (Ruck 2007) 1.0 ± 0.3 (Konig 1990)

No significant difference was observed in the photoproduct lifetime between subsequent acquisitions during this experiment, however a significant difference was found between the first and second acquisitions from the main fluorescence peak for both Photofrin® and PpIX (See Tables 3.1 and 3.1, Figures 3-8 to 3-11), which may be the effects of quenching with oxygen. There was no significant lifetime difference observed between the second and third acquisitions.

Ruck *et al.* reported that monomeric Photofrin® decayed with an average lifetime of 13.3 ± 0.3 ns in human HepG2 cells, while aggregates and photoproducts, which fluoresce at slightly longer wavelengths, decayed with a shorter average lifetime of 8.0 ± 0.6 ns (Ruck 2007). Konig *et al.* also documented the formation of Photofrin® photoproducts; they measured fluorescence lifetimes of 13.2 ± 2.0 ns and 1.0 ± 0.3 ns in mice bearing solid, subcutaneous EhrIich carcinoma. The long component was attributed to Photofrin® monomers and the short lifetime to aggregates (Konig 1990). Additionally, studies by Schneckenburger *et al.* concerning the fluorescence lifetimes of porphyrins such as Photofrin® and a similar compound, Photosan, in various cell types found three components to the decay: a slow component of 11 to 14 ns attributed to monomeric porphyrin, a medium component of 2 to 3 ns attributed to dimers, and a fast component of 0.1 to 0.3 ns attributed to aggregates (Schneckenburger 1992, Schneckenburger 1993). The results of this thesis have shown that localized Photofrin fluorescence in cells decays monoexponentially with an average lifetime of 7.8 ± 0.5 ns over the main fluorescence peak and 5.1 ± 0.4 ns over the photoproduct/aggregate peak (see Figure 3-8 and Table 4.1), which is significantly different from these reports. It is, however, similar to the change in lifetime between solution and in cells exhibited by ALA-PpIX. Kress *et al.* investigated ALA-induced PpIX in rat epithelial cells, and found a fluorescence lifetime of 7.44 ± 0.56 ns for the main peak and 3.6 ± 0.46 ns for the photoproduct peak; in a chorioallantoic membrane (CAM) model system,

lifetimes of 18 to 20 ns and 6 ns were measured for the main and photoproduct peaks respectively; additionally, lifetimes between 12.1 and 14.5 ns were found for the main peak in calf aorta endothelial cells (Kress 2003). Konig *et al.* investigated tumours in nude mice and found lifetimes of 17 ns and 5 ns for the main and photoproduct peaks respectively (Konig 1993). Theodossiou *et al.* found a lifetime of 5.4 ns over the photoproduct peak in PAM 212 cells (Theodossiou 2002). Results in this thesis for PpIX fall into the range represented by these experiments (see Figure 3-10 and Table 4.1). These variations demonstrate that photosensitizers' lifetimes change significantly when bonded to intracellular components, indicating that molecular binding plays a significant role in determining fluorescence lifetime. It can be speculated that the short lifetime measured in cells for Photofrin® may be a result of a high concentration of the drug accumulated in the mitochondria, resulting in self-quenching, however this hypothesis requires further investigation. This could be accomplished by imaging groups of cells incubated with several different concentrations of Photofrin®, spanning a large concentration range, to see whether or not an increase in concentration is correlated with a shortening of measured lifetime. It would also be instructive to perform co-localization studies for each concentration, as previously described, to observe drug localization as concentration increases.

The long-term goal of this study is towards real-time dosimetry using fluorescence lifetime information, seeking to determine whether or not fluorescence lifetime information could be useful in indicating photosensitizer

information, and whether or not the lifetime will correlate to changes the photosensitizer might undergo, such as the production of photoproducts or after photobleaching. In Chapter 3, it was demonstrated that the fluorescence lifetimes of Photofrin® and PpIX are both significantly longer than that of the cellular autofluorescence, indicating that fluorescence lifetime information would not be subject to interference from endogenous cellular fluorescence. Also encouraging is the fact that fluorescence lifetimes are not affected by influences the local cellular environment may have on extinction coefficient spectrum and quantum yield, or the absorption of emitted fluorescence by various chromophores which affect steady-state measurements, as previously mentioned. Photobleaching also does not affect the fluorescence lifetime. These indications suggest that fluorescence lifetime information would be useful in tracking photosensitizer concentration.

The lifetimes of photoproducts and aggregates have also been considered, and have been noted to be significantly shorter than the main fluorescence. It is speculated that the lifetimes found during one channel FLIM with the broad spectral window were mostly due to photoproducts, as the acquisition times were long, and considerable photoproduct generation could have occurred in that time. Consequences of high concentrations have also been discussed, noting that high concentrations of drug in the mitochondria could lead to self-quenching and a shorter apparent lifetime.

4.2 Excitation Modes – One and Two Photon Excitation

Two-photon excitation holds promise for applications in diagnosis, dosimetry, and PDT of small or exact volumes, as is the case with treatment of age-related macular degeneration, which affects the retina (Wilson 2006). This is largely because the nonlinear interaction is limited to the two-photon excitation volume, which allows for treatment volumes on the order of femtolitres, minimizing damage to adjacent healthy tissue (Wilson 2006). The independence of emission spectra on excitation wavelength follows Kasha's rule. Upon excitation into higher vibrational levels, excess energy dissipates nonradiatively, and the fluorophore is left in the lowest vibrational level of the first excited singlet state. It is the radiative transition from this level that results in fluorescence (Lakowicz 1999). Though the one-photon and two-photon absorption spectra may differ, sometimes substantially for a given fluorophore, the emission spectrum usually does not change significantly (Lakowicz 1999). Wilson *et al.* noted that after internal conversion reduces the fluorophore to the first excited singlet level, photophysical and photochemical processes are identical for one-photon and two-photon excitation (Wilson 2006). The fluorescence lifetime hence does not change with the type of excitation, which is confirmed by the streak camera based measurements under single and two-photon excitations.

4.3 Cellular Binding of Photosensitizers

Large differences were seen between the fluorescence lifetimes of the photosensitizers measured in solutions, and those of the photosensitizers measured in cells. Molecular binding is one of the factors that influences fluorescence lifetime, so it was expected that the lifetimes would change depending on the intracellular structures the photosensitizers were bound to, *e.g.* the membranes of the mitochondria. From the co-localization experiment with MitoTracker Green and the spatially resolved FLIM images, both photosensitizers appear to be accumulating, for the most part, in the mitochondria at the concentrations used in these experiments. The nature of the tissue or cells under investigation also seems to influence the fluorescence lifetime, as seen in the literature values presented in Table 4.1, especially for PpIX. One possible explanation for this observation is that mitochondria may differ between cell types, a theory that has been suggested (Hsueh-Meei 2004). Mitochondrial membrane potential, which has been linked to processes such as calcium uptake, production of reactive oxygen species and import of proteins into the mitochondria, has been shown to differ between different cell types, though the root cause of this observation is unknown (Hsueh-Meei 2004). As fluorescence lifetime is known to be influenced by ion concentrations (Wang 2007), it is conceivable that this may influence the observed lifetime of photosensitizers localized in the mitochondria.

4.4 Other Applications for Fluorescence

Fluorescence lifetime imaging with these photosensitizers could also be used for tumour imaging and diagnosis due to the selective uptake of the drugs by malignant tissue. For example, it has been observed that levels of ALA-induced PpIX in normal brain tissue are quite low, and that various factors such as the defective blood-brain barrier and different activity of the heme synthesis pathway contribute to the preferential accumulation of ALA-PpIX in certain brain tumours (Bogaards 2004). Stummer *et al.* assessed the effectiveness of fluorescence-guided resection of malignant gliomas using ALA-induced PpIX, which relies on the sufficient accumulation of fluorescent porphyrins in malignant tissue (Stummer 2006). The use of Photofrin® in fluorescence-guided tumour resection has also been discussed (Yang 2003). One limitation of these steady-state fluorescence based methods is the possible presence of the photosensitizer in surrounding normal tissue, which would result in the resection of healthy tissue. This also provides motivation for the characterization of fluorescence lifetimes in cells. Konig *et al.* determined that significant differences in fluorescence lifetime existed between normal peritumoural tissue and tumour tissue when treated with Photofrin®, and resolved that aggregates accumulated preferentially in tumour tissue (Konig 1990). Tumour imaging using fluorescence lifetimes could therefore provide another level of discrimination between malignant and normal tissue, beyond merely the degree of preferential accumulation.

4.5 Pulse Pile-up Effects

For time-domain measurements, it is desirable to excite the sample with laser pulses that are much farther apart than the lifetime of the sample (Lakowicz 1999). In the fluorescence lifetime imaging experiments in this study, an 80 MHz repetition rate excitation was used. In this case, the pulse period of the laser (12.5 ns) was similar to the lifetimes of the photosensitizers being measured. While this would affect the amplitudes for a biexponential fit, it would not influence the measured fluorescence lifetime, as shown below. Consider a biexponential decay as,

$$y(t) = Ae^{-\frac{t}{B}} + Ce^{-\frac{t}{D}} \tag{4.1}$$

where A and C are the pre-exponential weightings and B and D are the decay constants. Now consider the resulting decay if n identical y(t) decays were overlapped on top of each other with a period of Δt, which corresponds to the period of the laser and is equal to the inverse of the frequency,

$$y_n(t) = \left[Ae^{-\frac{t}{B}} + Ce^{-\frac{t}{D}} \right] + \left[Ae^{-\frac{t+\Delta t}{B}} + Ce^{-\frac{t+\Delta t}{D}} \right] + \ldots + \left[Ae^{-\frac{t+n\Delta t}{B}} + Ce^{-\frac{t+n\Delta t}{D}} \right] \tag{4.2}$$

The exponentials can be separated into exponentials containing only -t/τ terms and those containing only factors of –Δt/τ, where τ represents B or D. Like terms can then be collected, giving the following equation,

$$y_n(t) = A\left[1 + e^{-\frac{\Delta t}{B}} + \ldots + e^{-\frac{n\Delta t}{B}} \right] e^{-\frac{t}{B}} + C\left[1 + e^{-\frac{\Delta t}{D}} + \ldots + e^{-\frac{n\Delta t}{D}} \right] e^{-\frac{t}{D}} \tag{4.3}$$

$$y_n(t) = A\left[\sum_{n=0}^{\infty} e^{-\frac{n\Delta t}{B}}\right] e^{-\frac{t}{B}} + C\left[\sum_{n=0}^{\infty} e^{-\frac{n\Delta t}{D}}\right] e^{-\frac{t}{D}} \qquad (4.4)$$

As n approaches infinity, the sum terms converges asymptotically to constant values (see Figure 4-3). The sum terms are not time dependent, and thus become a part of the constant term which gives the amplitude for each exponential. The time dependent terms, however, remain the same as for the original decay expression, y(t).

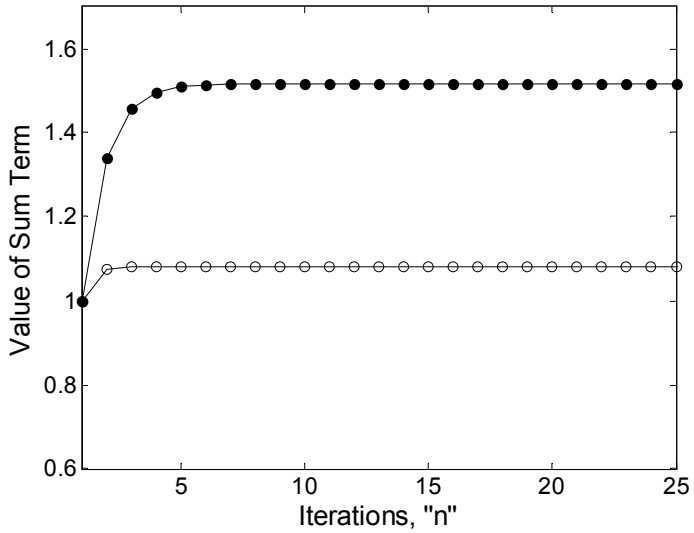

Figure 4-3 Converging sum terms from Equation 4.4. The filled circles show the convergence for the sum term corresponding to the first exponential, and the open circles show the convergence for the sum term corresponding to the second exponential. As can be seen, both sum terms converge asymptotically to constant values, which are essentially reached within the first few iterations. The values for A = 0.25, B = 4.8 ,C = 0.75 and D = 11.6 were taken from the results from the solution experiments with Photofrin® as described in Chapter 2.

This conclusion assumes only one decay is present after each pulse; in fact, since many molecules in a sample are excited multiple decays are present after each pulse. If all fluorophore molecules share the same fluorescence lifetime, then the probability of emitting a fluorescent photon at any given time

post-excitation is the same for each molecule. If all molecules are excited at the same time, and their fluorescence lifetimes are the same, then the fact that multiple decays are present does affect the above argument. It should also be noted that the above calculation is based upon the assumption that the individual decay dynamics of each pulse remains unchanged. This assumption can be satisfied only if photobleaching and/or other photodynamic processes are not significant. Therefore, a lower repetition rate ultrafast source is always desired.

4.6 Concluding Statements

In summary, Photofrin® and ALA-induced PpIX have been imaged using FLIM *in vitro* in MLL cells. Fluorescence lifetimes of both photosensitizers were found to be significantly shorter when localized in cells than when measured in solutions, suggesting that photosensitizers' lifetimes go through significant changes when bonded to intracellular components, therefore one should use caution when interpreting fluorescence lifetime experiment results. On the other hand, these changes in lifetime provide opportunities to quantitatively measure and monitor the binding states of the photosensitizers and their microenvironment, which may be used in real-time PDT dosimetry, as well as for diagnostic purposes.

This work has shown that fluorescence lifetimes of photosensitizers and their photoproducts can be measured in live cells. The application of fluorescence lifetime information to estimations of local tissue concentration have been

discussed, as well as the various advantages the use of fluorescence lifetime information would offer in terms of autonomy from various sources of interference that affect purely intensity-based measurements. The logical next step in this investigation is the analysis and characterization of these photosensitizers in various tissues under typical PDT conditions. Eventually, a time-domain spectroscopy apparatus developed for and directed towards clinical applications would need to be implemented, as the ultimate goal of this endeavor is the real-time clinical use of fluorescence lifetime measurements for dosage monitoring. It is hoped that this work has helped to provide a baseline for future investigations into the use of fluorescence lifetime as a means of determining fluorophore concentration in cells and tissue.

Bibliography

American Cancer Society. (2007) [Online]. Treatment Topics and Resources: Symptoms and Side Effects. Available: www.cancer.org/docroot/mbc/mbc_2_Side_Effects.asp Jan 7, 2007 [date accessed]

Axcan Pharma Inc. (2005) [Online]. PHOTOFRIN® Sterile porfimer sodium for injection, for intravenous use, antineoplastic photosensitizing agent. Available: http://www.axcan.com/pdf/photofrin.pdf Feb 18, 2008 [date accessed].

Becker, W., *The bh TCSPC Handbook*, Becker & Hickl GmbH, 2005

Becker & Hickl GmbH, *User Handbook: Leica MP-FLIM and D-FLIM: Fluorescence lifetime microscopy systems based on bh TCSPC technique*, Becker & Hickl GmbH , 2006

Bissonette, R., Bergeron, A., Liu, Y., "Large surface photodynamic therapy with aminolevulinic acid: treatment of actinic keratoses and beyond", *J. Drugs Dermatol.*, **3(1 Suppl)**, S26-31, 2004

Bogaards, A., Varma, A., Collens, S.P., Lin, A., Giles, A., Yang, V.X.D., Bilbao, J.M., Lilge, L.D., Muller, P.J., Wilson, B.C., "Increased brain tumor resection using fluorescence image guidance in a preclinical model", *Lasers in Surgery and Medicine*, **35**, 181-190, 2004

Borlinghaus, R., Kuschel, L. "Spectral fluorescence lifetime imaging microscopy: new dimensions with Leica TCS SP5" *Nature Methods*, **3**, iii-iv, October 2006

Brancaleon, L., Magennis, S.W., Samuel, I.D.W., Namdas, E., Lesar, A., Moseley, H. "Characterization of the photoproducts of protoporphyrin IX bound to human serum albumin and immunoglobulin G", *Biophysical Chemistry*, **109**, 351-360, 2003

Calzavara-Pinton, P.G., Venturini, M., Sala, R., "Photodynamic therapy: update 2006, Part 1: Photochemistry and photobiology", *European Academy of Dermatology and Venereology*, **21**, 293-302, 2007

Canadian Cancer Society (2007) [Online]. Canadian Cancer Statistics 2007. Available: http://www.cancer.ca/vgn/images/portal/cit_86751114/36/15/1816216925cw_2007stats_en.pdf Mar 8, 2008 [date accessed]

Canpolat, M., Mourant, J.R., "Monitoring photosensitizer concentration by use of a fiber-optic probe with a small source-detector separation," *Appl Opt*, **39**, 6508-6514, 2000a

Chen, Y., Periasamy, A., "Characterization of two-photon excitation fluorescence lifetime imaging microscopy for protein localization", *Microscopy Research and Technique*, **63**, 72-80, 2004

Chwilkowska, A., Saczko, J., Modrzycka, T., Marcinkowska, A., Malarska, A., Bielwwicz, J., Patalas, D., Banas, T., "Uptake of photofrin II, a photosensitizer used in photodynamic therapy, by tumour cells *in vitro*", *Acta Biochimica Polonica*, **50(2)**, 509-513, 2003

Claydon, P.E., and Ackroyd, R., "5-aminolaevulinic acid-induced photodynamic therapy and photodetection in Barrett's esophagus," *Diseases of the Esophagus*, **17**, 205-212, 2004

Cubeddu, R., Ramponi, R., Bottiroli., "Time-resolved fluorescence spectroscopy of hematoporphyrin derivatives in micelles", *Chemical Physics Letters*, **109(4)**, 439-442, 1986

Cubeddu, R., Comelli, D., D'Andrea, C., Taroni, P., Valentini, G., "Time-resolved fluorescence imaging in biology and medicine" *Journal of Physics D: Applied Physics*, **35**, R61-R76, 2002

Diamond, K.R., Patterson, M.S., and Farrell, T.J., "Quantification of fluorophore concentration in tissue-simulating media by fluorescence measurements with a single optical fiber," *Appl. Opt.* **42(13)**, 2436-2442, 2003

Diamond, K.R., "Quantification of fluorophore concentration and fluorescence quantum tield in tissue simulating phantoms and in vivo by fluorescence spectroscopy", Ph.D. dissertation, University of McMaster, Hamilton, ON, Canada, 2004

Diamond, K.R., Malysz, P.P., Hayward, J.E., Patterson, M.S., "Quantification of fluorophore concentration *in vivo* using two simple fluorescence-based measurement techniques," *Journal of Biomedical Optics*, **10(2)**, 024007-1 – 024007-10, 2005

Dougherty, T.J., Gomer, C.J., Henderson, B.W., Jori, G., Kessel, D., Korbelik, M., Moan, J., Peng, Q., "Photodynamic therapy," *Journal of the National Cancer Institute*, **90(12)**, 889-905, 1998

Dougherty, T.J., Levy, J.G., "Photodynamic Therapy (PDT) Clinical Applications" in *Biomedical Photonics Handbook*, Vo-Dinh, T., Ed. New York: CRC Press, 2003, pp 38-4

Dowling, K., Dayel, M.J., Lever, M.J., French, P.M.W., Hares, J.D., Dymoke-Bradshaw, A.K.L., "Fluorescence lifetime imaging with picosecond resolution for biomedical applications", *Opt. Lett.*, **23(10)**, 810-812, 1998

Dysart, J.S., Patterson, M.S., "Characterization of Photofrin photobleaching for singlet oxygen dose estimation during photodynamic therapy of MLL cells *in vitro*", *Phys. Med. Bio.*, **50**, 2597-2616, 2005

Dysart, J.S., Patterson, M.S., "Photobleaching kinetics, photoproduct formation, and dose estimation during ALA induced PpIX PDT of MLL cells under well oxygenated and hypoxic conditions:, *Photochemical & Photobiological Sciences*, **5**, 73-81, 2006

Egner, A., Hell, S.W., "Time multiplexing and parallelization in multifocal multiphoton microscopy", *J. Opt. Soc. Am. A*, **17(7)**, 1192-1201, 2000

Elson, D.S., Siegel, J., Webb, S.E.D., Leveque-Fort, S., Parsons-Karavassilis, D., Cole, M.J., French, P.M.W., Davis, D.M., "Wide-field fluorescence lifetime imaging with optical sectioning and spectral resolution applied to biological samples", *Journal of Modern Optics*, **49(5/6)**, 985-995, 2002

Glanzmann, T., Ballini, J.P., van der Bergh, H., Wagnieres, G., "Time-resolved spectrofluorometer for clinical tissue characterization during endoscopy" *Review of Scientific Instruments*, **70(10)**, 4067-4077, 1999

Henderson, B.W., Gollnick, S.O., "Mechanistic Principles of Photodynamic Therapy" in *Biomedical Photonics Handbook*, Vo-Dinh, T., Ed. New York: CRC Press, 2003, pp 36-2

Hsueh-Meei, H., Fowler, C., Zhang, H., Gibson, G.E., "Mitochondrial heterogeneity within and between different cell types," *Neurochemical Research*, **29(3)**, 651-658, 2004

Kleinsmith, L.J., *Principles of Cancer Biology*, San Francisco: Benjamin Cummings 2006, pp1-43, 208-217

Kondo, M., Hirota, N., Takaoka, T. and Kajiwara, M., Heme-biosynthetic enzyme activities and porphyrin accumulation in normal liver and hepatoma cell lines of rat, *Cell Biol. Toxicol.* **9**, 95-105, 1993

Konig, K., Wabnitz, H., Dietel, W., "Variation in the fluorescence decay properties of haematoporphyrin derivative during its conversion to photoproducts", *Journal of Photochemistry and Photobiology B: Biology*, **8**, 103-111, 1990

Konig, K, Schneckenburger, H., Ruck, A., Steiner, R., "In vivo photoproduct formation during PDT with ALA-induced endogenous porphyrins", *J. Photochem. Photobiol. B: Biol*, **18**, 287-290, 1993

Kress, M., Meier, T., Steiner, R., Dolp, F., Erdmann, R., Ruck, A., "Time-resolved microspectrofluorometry and fluorescence lifetime imaging of photosensitizers using picosecond pulsed diode lasers in laser scanning microscopes", *J. Biomed. Opt*, **8(1)**, 26-32, 2003

Lakowicz, Joseph R., *Principles of Fluorescence Spectroscopy 2nd Ed*. New York: Springer Science+Business Media, 1999

Lee, C. C., Pogue, B. W., Strawbridge, R. R., Moodie, K. L., Bartholomew, L. R., Burke, G. C., and Hoopes, P. J., ''Comparison of photosensitizer (AlPcS2) quantification techniques: in situ fluorescence microsampling versus tissue chemical extraction,'' *Photochem. Photobiol.* **74**, 453–460, 2001

Magde, D., Wong, R., Seybold, PG., "Fluorescence quantum yields and their relation to lifetimes of rhodemine 6G and Fluorescin in nine solvents: improved absolute standards for quantum yields:, *Photochemistry and Photobiology*, **75(4)**, 327-334, 2002

Mourant, J. R., Johnson, T. M., Los, G., and Bigio, I. J. , ''Non-invasive measurement of chemotherapy drug concentrations in tissue: preliminary demonstrations of in vivo measurements,'' *Phys. Med. Biol.* **44**, 1397–1417, 1999

Panjehpour, M., Sneed, R. E., Frazier, D. L., Barnhill, M. A., O'Brien, S. F., Harb, W., and Overholt, B. F., ''Quantification of phthalocyanine concentration in rat tissue using laser-induced fluorescence spectroscopy,'' *Lasers Surg. Med.* **13**, 23–30, 1993

Pelengaris, S., Khan, M., "Introduction" in *The Molecular Biology of Cancer*, Pelengaris, S., Khan, M., Ed. Malden: Blackwell Publishing, 2006, pp 1-34

Periasamy, A., Wodnicki, P., Wang, X.F., Kwon, S., Gordon, G.W., Herman, B., "Time-resolved fluorescence lifetime imaging microscopy using a picosecond pulsed tunable dye laser system", *Rev. Sci. Instrum.*, **67(10)**, 3722-3731, 1996

Pitts, J.D., Mycek, M.A., "Design and development of a rapid acquisition laser-based fluorometer with simultaneous spectral and temporal resolution" *Rev. Sci. Instru.*, **72(7)**, 3061-3072, 2001

Potter, W.R., Mang, T.S., "Photofrin II levels by *in vivo* fluorescence photometry," *Porphyrin Localization and Treatment of Tumors*, **101**, 177-186, 1984

Richards-Kortum, R., Sevick-Muraca, E., "Quantitative optical spectroscopy for tissue diagnosis", *Annu. Rev. Rhys. Chem.*, **47**, 555-606, 1996

Ruck, A., Hulshoff, C.H., Kinzler, I., Becker, W., Steiner, R., "SLIM: A new method for molecular imaging", *Microscopy Research and Technique*, **70**, 485-492, 2007

Schaferling, M., "Luminescence lifetime-based imaging of sensor arrays for high-throughput screening applications", *Springer Ser Chem Sens Biosens*, **3**, 45-92, 2005

Schneckenburger, H., Seidlitz, H., Stettmaier, K., Wessels, J., "Intracellular polarization, picosecond kinetics and light-induced reactions of photosensitizing porphyrins,: *Opt. Eng*. **31**, 1482-1486, 1992

Schneckenburger, H., König, K., Kunzi-Rap,p K,. Westpal-Frosch, C., Ruck, A., "Time-resolved in-vivo fluorescence of photosensitizing porphyrins," *J. Photochem. Photobiol*. **21**, 143-147, 1993

Siegal, J., Elson, D.S., Webb, S.E.D., Parsons-Karavassilis, D., Leveque-Fort, S., Cole, M.J., Lever, M.J., French, P.M.W., Neil, M.A.A., Juskaitis, R., Sucharoc, L.O., Wilson, T., "Whole-field five-dimensional fluorescence microscopy combining lifetime and spectral resolution with optical sectioning", *Opt. Lett.*, **26(17)**, 1338-1340, 2001

Stummer, W., Picjlmeier, U., Meinel, T., Wiestler, O.D., Zanella, F., Reulen, H.J., "Fluorescence-guided surgery with 5-aminolevulinic acid for resection of malignant glioma: a randomised controlled multicentre phase III trial", *Lancet Oncology*, **7(5),** 392-401, 2006

Tang, J., Zeng, F., Savage, H., Ho, P.P., Alfano, R.R., "Laser irradiative tissue probed in situ by collagen 380-nm fluorescence imaging", *Lasers in Surgery and Medicine*, **27**, 158-164, 2000

Terpetschnig, E., Jameson, D.M., Barbieri, B., "Frequency-domain spectroscopy using 280-nm and 300-nm LEDs," ISS (2008) [Online]. Available: http://www.iss.com/resources/app2/ Mar 20, 2008 [date accessed]

Theodossiou, T, MacRobert, A.J., "Comparison of the Photodynamic Effect of Exogenous Photoprotoporphyrin and Protoporphyrin IX on PAM 212 Murine Keratinocytes," *Photochemistry and Photobiology*, **76(5)**, 530-537, 2002

Thomas, A.L., Sharma, R.A., Steward, W.P., "Treatment of Cancer: Chemotherapy and Radiotherapy" in *The Molecular Biology of Cancer*, Pelengaris, S., Khan, M., Ed. Malden: Blackwell Publishing, 2006, pp 444-463

Torricelli, A., Pifferi, A., Taroni, P., Glambattistelli, E., Cubeddu, R., "In vivo optical characterization of human tissues from 610 to 1010 nm by time-resolved reflectance spectroscopy", *Physics in Medicine and Biology*, **46**, 2227-2237, 2001

US Food and Drug Administration: Center for Drug Evaluation and Research. (2007) [Online]. FDA Oncology Tools Product Label Details in Conventional Order for porfimer sodium. Available: www.accessdata.fda.gov/scripts/cder/onctools/labels.cfm?GN=porfimer%20sodium Jan 7, 2007 [date accessed]

Vishwanath, K., Pogue, B., and Mycek, M.A., ''Quantitative fluorescence lifetime spectroscopy in turbid media: comparison of theoretical, experimental and computational methods,'' *Phys. Med. Biol.* **47**, 3387–3405, 2002

Vishwanath, K., Mycek, M.A., "Do fluorescence decays remitted from tissues accurately reflect intrinsic fluorophore lifetimes?", *Optics Letters*, **29(13)**, 1512-1514, 2004

Wang, H.P., Nakabayashi, T., Tsujimoto, K., Miyauchi, S., Kamo, N., Nobuhio, O., "Fluorescence lifetime image of a single halobacterium," *Chemical Physics Letters*, **422**, 441-444, 2007

Weersink, R., Patterson, M.S., Diamond, K., Silver, S., Padgett, N., "Noninvasive measurement of fluorophore concentration in turbid media using a simple fluorescence/reflectance ratio technique", *Appl. Opt.*, **40(34)**, 6389-6395, 2001

Williams, G., Pazdur, R., Temple, R., "Assessing tumor-related signs and symptoms to support cancer drug approval" *Journal of Biopharmaceutical Statistics*, **14(1)**, 5-21, 2004

Wilson, B.C., Patterson, M.S., "The physics of photodynamic therapy", *Phys. Med. Biol.*, **31(4)**, 327-360, 1986

Wilson, B.C., Karotki, A., Khurana, M., Lepock, J.R., "Simultaneous two-photon excitation of Photofrin in relation to photodynamic therapy", *Photochemistry and Photobiology*, **82**, 443-452, 2006

Yang, V.X.D., Muller, P.J., Herman, P., Wilson, B.C., "A multispectral fluorescence imaging system: design and initial clinical tests in intra-operative photofrin-photodynamic therapy of brain tumors", *Lasers in Surgery and Medicine*, **32**, 224-232, 2003